# Spike oscillations

J. Mark Heinzle,[1,*] Claes Uggla,[2,†] and Woei Chet Lim[3,‡]

[1]*Faculty of Physics, Gravitational Physics, University of Vienna, Boltzmanngasse 5, 1090 Vienna, Austria*
[2]*Department of Physics, University of Karlstad, 65188 Karlstad, Sweden*
[3]*Department of Mathematics, University of Waikato, Private Bag 3105, Hamilton, New Zealand and Albert-Einstein-Institut,*
*Am Mühlenberg, 14476 Potsdam, Germany*

According to Belinskiǐ, Khalatnikov and Lifshitz (BKL), a generic spacelike singularity is characterized by asymptotic locality: Asymptotically, toward the singularity, each spatial point evolves independently from its neighbors, in an oscillatory manner that is represented by a sequence of Bianchi type I and II vacuum models. Recent investigations support this conjecture but with a modification: Apart from local BKL behavior there also exists formation of spatial structures ("spikes") at, and in the neighborhood of, certain spatial surfaces that break asymptotic locality; the complete description of a generic spacelike singularity involves *spike oscillations*, which are described by sequences of Bianchi type I and certain *inhomogeneous* vacuum models. In this paper we describe how BKL and spike oscillations arise from concatenations of exact solutions in a Hubble-normalized state space setting, suggesting the existence of hidden symmetries and showing that the results of BKL are part of a greater picture.

## I. INTRODUCTION

This paper is part of a research program on generic spacetime singularities. It is concerned with *spike oscillations*, a missing piece in the description of the asymptotic dynamics of spacetimes toward a generic spacelike singularity.

In research beginning in the 1960s, Belinskiǐ, Khalatnikov and Lifshitz (BKL) claimed to have constructed an approximate general solution to Einstein's field equations in the vicinity of a spacelike ("cosmological") singularity [1–3]. The central assumption of BKL is that the asymptotic dynamics is *local* in the sense that each spatial point evolves toward the singularity individually and independently of its neighbors as a spatially homogeneous model. In addition, BKL gave heuristic arguments that suggested that perfect fluid models with soft equations of state, such as dust or radiation, are asymptotically *vacuum dominated*, i.e., asymptotically toward the singularity the spacetime geometry is not influenced by the matter content. Moreover, the BKL conjecture stated that for generic asymptotically vacuum dominated models the evolution of each spatial point in the vicinity of the singularity is approximated by a sequence of vacuum Bianchi type I solutions (i.e., Kasner solutions) mediated by vacuum Bianchi type II solutions, where the latter determine a discrete "Kasner map" with chaotic properties [4–21]. In general, the Kasner map generates infinite sequences of Kasner states, and BKL argued that these sequences describe *oscillatory* temporal behavior toward a generic spacelike singularity.

Based on earlier work by Kirillov and Kochnev [22] and Montani [23] Belinskiǐ pointed out in 1992 that the

independent evolution of different time lines (due to the locality assumption) leads to a lack of temporal synchronization of oscillations, and hence spatial structure formation, reminiscent of turbulence, takes place. This made Belinskiǐ himself, as well as others, start to question if the locality assumption of BKL is consistent [24]; see also Ref. [19] and references therein.

In 1993 Berger and Moncrief numerically studied vacuum $G_2$ models (i.e., models with two spacelike commuting Killing vectors [7]) with $T^3$ topology, so-called $T^3$ Gowdy models [25,26], and observed the development of large spatial derivatives near the singularity, which they called "spiky features" [27]. Furthermore, based on work by Grubišić and Moncrief of the same year [28], these features were tied to a condition at isolated spatial surfaces that could be imposed on a formal expansion of the Gowdy metric near the singularity.[1]

Toward the end of the 1990s, Berger, Moncrief and co-workers had found further numerical evidence that the BKL picture seemed to be correct generically in vacuum $G_2$ spacetimes, and even in spacetimes with only one spacelike Killing vector, but that there were difficulties at exceptional isolated spatial surfaces [29–32]; see also Ref. [10] and references therein. About the same time, Hern independently resolved individual spatially spiky features to high numerical accuracy, although for short time scales [33,34].

---

*mark.heinzle@univie.ac.at
†claes.uggla@kau.se
‡wclim@waikato.ac.nz

---

[1]Due to the symmetries of $G_2$ models, fields only depend on time and a single spatial coordinate; hence, two-dimensional symmetry surfaces, defined by a fixed value of this spatial coordinate, are often referred to as spatial points in the $G_2$ literature. However, since our ultimate objective is generic singularities (in spacetimes without symmetries), and because in that context this nomenclature is inappropriate, we will refrain from referring to surfaces as points.

A significant analytic step toward an understanding of spiky features in $T^3$ Gowdy models was accomplished in 2001 by Rendall and Weaver [35]. They applied a solution generating technique and Fuchsian methods in Refs. [36,37] to produce asymptotic expansions for "spikes," which they referred to as "true" or "false" spikes, where false spikes where shown to be gauge artifacts. The work on spiky features in Gowdy spacetimes by Rendall and Weaver was followed up by Garfinkle and Weaver in 2003 who used two different complementary numerical techniques [38]. In particular they studied so-called "high velocity spikes" and found that they eventually transform into "low velocity spikes." The term velocity as well as other diagnostic tools for describing and understanding asymptotic features associated with singularities are defined and discussed in Appendix D. For further and recent primarily analytic work on $T^3$ Gowdy models we refer to the review [39] and references therein.

Up to this point, the framework for studying singularities in inhomogeneous spacetimes had been dominated by the metric approach, as exemplified by the work of BKL, and the Hamiltonian approach used by Moncrief and co-workers. However, at the same time, the studies of spatially homogeneous models were dominated by the "Hubble-normalized" dynamical systems approach introduced by Wainwright and Hsu [40]. This led to substantial progress [7,41,42], which in turn has resulted in the recent remarkable developments about generic singularities in spatially homogeneous models; see Refs. [43–48]. In 2003 in an attempt to generalize this framework to a general inhomogeneous context, Uggla *et al.* [49] (UEWE) recast Einstein's field equations into an infinite dimensional dynamical system by means of Hubble-normalized scale-invariant variables. This resulted in a more specific and precise formulation of the BKL conjecture in terms of the asymptotically regularized field equations on an asymptotically bounded state space. The approach in UEWE was subsequently reformulated somewhat by means of a conformal transformation [50] which led to a geometric framework that was in turn specialized by means of a conformally Hubble-normalized Iwasawa frame by Heinzle *et al.* [51] to provide a link to work on cosmological billiards [52], and to establish the consistency of the BKL picture by means of dynamical systems methods.

Numerical studies based on the dynamical systems formulation in UEWE also gave support for the BKL picture generically [53,54], and provided evidence that the structure formation predicted by Belinskiĭ [24] is *not* a threat to the consistency of the BKL scenario, since it develops on superhorizon scale toward the singularity (see also Ref. [55]); i.e., horizons along time lines whose evolution is described by BKL behavior are shrinking faster than spatial gradients are increasing along them toward the singularity. However, the consistency of the billiard and BKL pictures does not exclude other behavior at generic

singularities. Numerical and heuristic arguments also suggested that there exist recurring temporal spike oscillations along certain time lines. These time lines correspond to spatial points that form two-dimensional *spike surfaces* and their spatially shrinking neighborhoods. The temporal spike oscillations are gauge invariant features that are distinct from BKL oscillations, as illustrated by the evolution of the Weyl scalars; in contrast to the BKL case, spatial derivatives contribute significantly to the Weyl scalars along the time lines of the spike surfaces (and in their shrinking neighborhoods), and in this sense oscillatory spike evolution is 'nonlocal'.

Based on the solution generating technique used by Rendall and Weaver to produce approximate solutions [35], in 2008 Lim was able to find a 1-parameter family of explicit (exact) inhomogeneous vacuum $G_2$ *spike solutions*, which are expressible in terms of elementary functions [56]. As suggested by the work in Refs. [53,54], these solutions form the building blocks for spike oscillations. This was further substantiated by Lim *et al.* in 2009 [57] where the analytic spike solutions found by Lim were numerically matched with high accuracy to actual $G_2$ solutions in the regime toward the singularity (at least for a small number of spike oscillations). Furthermore, Lim *et al.* managed to provide numerical evidence that showed that "higher order spike solutions," with several spike surfaces, could be described, locally and asymptotically, by the simpler "first order spike solutions" with a single spike surface. Hence the first order spike solutions seem to be the building blocks for describing spike oscillations in general (at least for the spiky non–BKL behavior discovered so far in numerical simulations), and it is therefore these solutions that we will focus on in this paper (for the influence of spike solutions on matter we refer to Ref. [58]).

In the BKL scenario, Bianchi type II vacuum solutions connect Kasner solutions, and for this reason we will refer to a Bianchi type II solution as a *transition* from one Kasner state to another. As a consequence this leads to "BKL oscillations" between different Kasner states. In terms of dynamical systems where the Kasner solutions are expressed as fixed points and the Bianchi type II vacuum solutions as "heteroclinic orbits", which by definition join two fixed points, this is made rigorous by *concatenation* of solutions into *heteroclinic chains* (BKL chains), i.e., joining of solutions by means of their asymptotics into chains of solutions connected via fixed points. Note that heteroclinic chains are not solutions of the Einstein equations themselves; however, concatenation of solutions to such chains is a mechanism that describes the asymptotic evolution of solutions approximately with increasing accuracy. In this context it is worth pointing out the recent developments in Bianchi types VIII and IX, which show that heteroclinic chains describe asymptotic dynamics in these models [43–48]. A goal of the present paper is to

show how the explicit spike solutions by Lim connect the (generalized) Kasner metrics in the Hubble-normalized state space picture. Thereby we obtain a network of *spike chains* that represent the asymptotic dynamics of solutions and thus the spike oscillations. Throughout this paper we focus on general vacuum $G_2$ models. There are reasons to believe that these models describe essential features of generic spacelike singularities, i.e., the general singularities that occur in models without symmetries [53,57]; we will return to this issue in the concluding remarks.

The paper is organized as follows. Section II provides a succinct overview of the $G_2$ models in the conformal ortho-normal (Iwasawa) frame approach. Section III is devoted to the essential building blocks of local BKL and nonlocal spike dynamics: Transitions. We discuss frame and curva-ture transitions and give a detailed account of the explicit high and low velocity spike solutions found by Lim tailored to our purposes and in the conformally Hubble-normalized picture. Section IV treats a special class of $G_2$ models, the orthogonally transitive $G_2$ models which comprises, e.g., the $T^3$ Gowdy models. We describe in detail how transitions can be concatenated to obtain *chains* of transitions that are relevant for the asymptotic dynamics of solutions. Finally, Sec. V treats the general $G_2$ case. In this case, concatenation leads to (in general) infinite BKL chains and spike chains that determine the oscillatory behavior of $G_2$ solutions toward the singularity. Section VI contains the conclusions together with a brief description and assessment of previous numerical results in view of our present analytical and numerical understanding. We also discuss connections between BKL and non–BKL behavior and give hints to underlying hidden asymptotic symmetries. The appendices contain a discussion of topological issues and a brief review of the results on $T^3$ Gowdy spacetimes; we stress that the "permanent" spiky features characteristic of the $T^3$ Gowdy case are replaced by transient recurrent features in the general $G_2$ case: spike oscillations.

## II. $G_2$ MODELS IN THE CONFORMAL ORTHONORMAL FRAME APPROACH

In this paper we study vacuum $G_2$ models, which are characterized by the existence of two spacelike commuting Killing vector fields. In symmetry-adapted local coordi-nates these Killing vectors are $\partial_x$ and $\partial_y$, which allows the metric to be written as

$$
\begin{aligned}
ds^2 = &-N^2(dx^0)^2 + e^{-2b^1}(dx + n_1 dy + n_2 dz)^2 \\
&+ e^{-2b^2}(dy + n_3 dz)^2 + e^{-2b^3}dz^2 = -N^2(dx^0)^2 \\
&+ e^{-2b^1}(dx - \bar{n}_1 dy + (-\bar{n}_2 + \bar{n}_1 \bar{n}_3)dz)^2 \\
&+ e^{-2b^2}(dy - \bar{n}_3 dz)^2 + e^{-2b^3}dz^2,
\end{aligned} \tag{1}
$$

where all functions depend on $x^0$ and the spatial coordinate $z$ alone, and where $n_1 = -\bar{n}_1$, $n_2 = -\bar{n}_2 + \bar{n}_1\bar{n}_3$, $n_3 = -\bar{n}_3$; for the first form of the line element see Ref. [59], while for

the second form see Refs. [32,60–62]. We refer to Appendix A for details and for a topological discussion. The first form of the line element provides an *Iwasawa* representation of the metric and is naturally associated with the orthonormal spatial (co-)frame $\{\omega^1, \omega^2, \omega^3\}$ determined by

$$
\begin{pmatrix} \omega^1 \\ \omega^2 \\ \omega^3 \end{pmatrix} = \begin{pmatrix} e^{-b^1} & 0 & 0 \\ 0 & e^{-b^2} & 0 \\ 0 & 0 & e^{-b^3} \end{pmatrix} \begin{pmatrix} 1 & n_1 & n_2 \\ 0 & 1 & n_3 \\ 0 & 0 & 1 \end{pmatrix} \begin{pmatrix} dx \\ dy \\ dz \end{pmatrix}, \tag{2a}
$$

which is the dual of the orthonormal spatial "Iwasawa frame" $\{e_1, e_2, e_3\}$ (see, e.g., Secs. 2 and 13 in Ref. [51]) given by

$$
\begin{pmatrix} e_1 \\ e_2 \\ e_3 \end{pmatrix} = \begin{pmatrix} e^{b^1} & 0 & 0 \\ 0 & e^{b^2} & 0 \\ 0 & 0 & e^{b^3} \end{pmatrix} \begin{pmatrix} 1 & \bar{n}_1 & \bar{n}_2 \\ 0 & 1 & \bar{n}_3 \\ 0 & 0 & 1 \end{pmatrix} \begin{pmatrix} \partial_x \\ \partial_y \\ \partial_z \end{pmatrix}. \tag{2b}
$$

Combining this spatial frame with $e_0 = N^{-1}\partial_t$ and $\omega^0 = Ndx^0$ yields an Iwasawa based orthonormal frame for the spacetime metric, i.e., $ds^2 = -\omega^0 \otimes \omega^0 + \delta_{\alpha\beta}\omega^\alpha \otimes \omega^\beta$, where we use Greek letters as spatial frame indices.

The area density of the symmetry surfaces is $R = e^{-b^1-b^2}$. Whenever the gradient of $R$ is timelike, it is possible to define time by choosing $R$ to be a prescribed monotone function, e.g., $R \equiv x^0$, or

$$
-\log R = b^1 + b^2 = t + t_0, \tag{3}
$$

for some constant $t_0$ (which is chosen to be $t_0 = 0$ unless stated otherwise). As shown in Refs. [60,63], for the $T^3$ case, $R \propto \exp(-t) \in (0, \infty)$ represents the maximal globally hyper-bolic development of initial data at $t = \text{const}$, where $t \to \infty$ represents the initial singularity; the only exception is the Taub (flat Kasner) solution. In the *area time gauge* (3), in the nomenclature of Ref. [64], the line element can be written as

$$
\begin{aligned}
ds^2 = &e^{-2b^3}(-\bar{\alpha}e^{-2t}dt^2 + dz^2) + e^{-2b^1}(dx + n_1 dy + n_2 dz)^2 \\
&+ e^{-2t+2b^1}(dy + n_3 dz)^2,
\end{aligned} \tag{4}
$$

where $\bar{\alpha} \neq 1$ in general.

An important subclass of the $G_2$ models are the *orthog-onally transitive* (OT) models; see Refs. [65,66] and p. 43 in Ref. [7]; we refer to Appendix A for details. In these models the coordinates can be adapted so that $n_2 = n_3 = 0$ and $\bar{\alpha} = 1$, which corresponds to setting the lapse function to

$$
\begin{aligned}
N &= -\exp(-[t + b^3]) = -\exp(-[b^1 + b^2 + b^3]) \\
&= -\sqrt{\det^{(3)} g}, \tag{5}
\end{aligned}
$$

where it is to be noted that the direction of time is toward the past singularity, as is the case throughout this paper. As seen, the metric in the OT case simplifies considerably, see also (45) and (D1).

In this paper we focus on analyzing and representing solutions by means of conformally Hubble-normalized Iwasawa adapted variables, see Ref. [50] and section 2 of Ref. [51], rather than the metric variables $b^1$, $b^2$, $b^3$ and $n_1$, $n_2$, $n_3$. The complete set of relations between the conformally Hubble-normalized variables and the metric variables are given in Appendix B; here we restrict ourselves to giving the relations for the key objects: The Hubble scalar, which is

one third of the derivative of the logarithm of the spatial volume density with respect to proper time, is given by

$$H = -\frac{1}{3}N^{-1}\partial_{x^0}(b^1 + b^2 + b^3), \tag{6}$$

while the conformally Hubble-normalized shear variables take the form

$$\Sigma_\alpha := \Sigma_{\alpha\alpha} = -1 - (HN)^{-1}\partial_{x^0}b^\alpha \qquad (\alpha = 1, 2, 3), \tag{7a}$$

$$\Sigma_{23} = \frac{1}{2}\exp(b^3 - b^2)(HN)^{-1}\partial_{x^0}n_3, \qquad \Sigma_{12} = \frac{1}{2}\exp(b^2 - b^1)(HN)^{-1}\partial_{x^0}n_1 \tag{7b}$$

so that $\Sigma_1 + \Sigma_2 + \Sigma_3 = 0$; note that $\Sigma_{31} = 0$, see Appendices A and B. We use Greek indices to refer to the components of tensors with respect to the conformally Hubble-normalized Iwasawa frame. In general a spatial orthonormal frame rotates with respect to a gyroscopically fixed spatial frame (which is a so-called Fermi-propagated frame). In the present approach, this spatial frame rotation is encoded in the functions $R_\alpha$, $\alpha = 1, 2, 3$, which, as a consequence of the Iwasawa parametrization, are tied to the off-diagonal shear components by

$$\Sigma_{23} = -R_1, \qquad \Sigma_{12} = -R_3, \qquad \Sigma_{31} = R_2 = 0; \tag{8}$$

see Ref. [51]. We choose to use $R_1$ and $R_3$ as independent variables, instead of $\Sigma_{23}$ and $\Sigma_{12}$. Note that $\Sigma_{23} = -R_1 = 0$ in the OT case; see Appendix B. Finally, it is of interest to also give the Hubble-normalized spatial commutator function $N_1(= N_{11})$:

$$N_1 = H^{-1}\exp(b^2 + b^3 - b^1)\partial_z n_1. \tag{9}$$

The Einstein vacuum equation in the conformal Hubble-normalized orthonormal frame approach is given in Appendix C.

In the following we will analyze $G_2$ vacuum models in terms of the conformally Hubble-normalized orthonormal frame variables. In particular, to illustrate the behavior of solutions, we will use projections onto $(\Sigma_1, \Sigma_2, \Sigma_3)$ space and monitor the behavior of $N_1$ along the arising trajectories.

## III. TRANSITIONS

In the Hubble-normalized approach a state space picture emerges which is central for the analysis of the (asymptotic) dynamics of $G_2$ models. The key structure on the boundary of the state space is the "Kasner circle" of fixed points which represents "generalized" Kasner metrics. These fixed points are connected by an intricate network of curves and families of curves representing generalized spatially homogeneous solutions and inhomogeneous solutions, which we denote by transitions in this context. The Kasner circle and the transitions turn out to be the building blocks of generic

oscillatory singularities of $G_2$ models (and beyond); see Sec. V.

### A. The Kasner circle

The Kasner, i.e., vacuum Bianchi type I, solution is usually given as

$$ds^2 = -d\tilde{t}^2 + \tilde{t}^{2p_1}d\tilde{x}^2 + \tilde{t}^{2p_2}d\tilde{y}^2 + \tilde{t}^{2p_3}d\tilde{z}^2,$$
$$(p_1 + p_2 + p_3 = 1 = p_1^2 + p_2^2 + p_3^2), \tag{10}$$

where the constants $p_1$, $p_2$, $p_3$ are known as the Kasner exponents. By making a constant transformation of the coordinates according to $\tilde{t} = \hat{c}^0{}_0\hat{t}$, $\tilde{x} = \tilde{c}^1{}_j\hat{x}^j$, $\tilde{y} = \tilde{c}^2{}_j\hat{x}^j$, $\tilde{z} = \tilde{c}^3{}_j\hat{x}^j$, the Kasner solution takes the form

$$ds^2 = -(\hat{c}^0{}_0 d\hat{t})^2 + \hat{t}^{2p_1}(\hat{c}^1{}_j d\hat{x}^j)^2 + \hat{t}^{2p_2}(\hat{c}^2{}_j d\hat{x}^j)^2$$
$$+ \hat{t}^{2p_3}(\hat{c}^3{}_j d\hat{x}^j)^2, \tag{11}$$

where the constants $\hat{c}^i{}_j$ are obtained by appropriately scaling $\tilde{c}^i{}_j$ with $\hat{c}^0{}_0$. The *generalized* Kasner metric is defined by letting the constants $p_\alpha$, $\hat{c}^0{}_0$ and $\hat{c}^i{}_j$ be arbitrary functions of the spatial coordinates. As a consequence this metric is not a solution of Einstein's field equations; its importance lies in its role as a building block in the description of the asymptotic dynamics of actual solutions. In the present context of $G_2$ models with Iwasawa parametrized metrics we have $\hat{c}^2{}_1 = \hat{c}^3{}_1 = \hat{c}^3{}_2 = 0$, and functions are functions of $z(= x^3)$ alone.

In Appendix B of Ref. [51], the conformal Hubble-normalized approach was used to derive the generalized Kasner metrics by perturbing away from the *local boundary* (which previously was called the silent boundary, see Refs. [67,68] for a discussion). The local boundary is an invariant boundary subset of the Hubble-normalized state space that is obtained by setting all Hubble-normalized spatial frame components (and hence spatial frame derivatives) to zero.[2] By construction, the equations induced by

---

[2]In the $G_2$ context the local boundary is obtained by setting $E_3 = 0$, and hence $E_3\partial_z = \boldsymbol{\partial}_3 = 0$, in Appendix C.

the field equations on the local boundary coincide with the equations describing spatially homogeneous models, where, however, constants of integration become spatial functions. Accordingly, the local boundary provides a well-defined state space setting for the BKL concept of "generalized spatially homogeneous metrics."

The structure on the local boundary that is of prime importance for our understanding of the asymptotic dynamics of solutions toward a singularity is the *Kasner circle* $K^\circ$. The Kasner circle is obtained by setting all Hubble-normalized variables to zero except the diagonal shear variables $\Sigma_1, \Sigma_2, \Sigma_3$. (In particular, the rotation variables $R_1, R_2, R_3$ are zero, i.e., the frame that is used is a Fermi-propagated frame). The equations then imply that the diagonal shear variables are constants in time but functions of the spatial coordinate(s). The single remaining (algebraic) equation on the local boundary is the Gauss constraint, which then characterizes $K^\circ$:

$$\Sigma_\alpha = \text{const} \quad \forall \, \alpha, \qquad \Sigma_1 + \Sigma_2 + \Sigma_3 = 0,$$
$$\Sigma^2 := \frac{1}{6}\Sigma_{\alpha\beta}\Sigma^{\alpha\beta} = \frac{1}{6}(\Sigma_1^2 + \Sigma_2^2 + \Sigma_3^2) = 1, \tag{12}$$

where $\Sigma_\alpha$ are related to the generalized Kasner exponents $p_\alpha$ according to

$$\Sigma_\alpha = 3p_\alpha - 1 \quad \forall \, \alpha, \quad p_1 + p_2 + p_3 = 1,$$
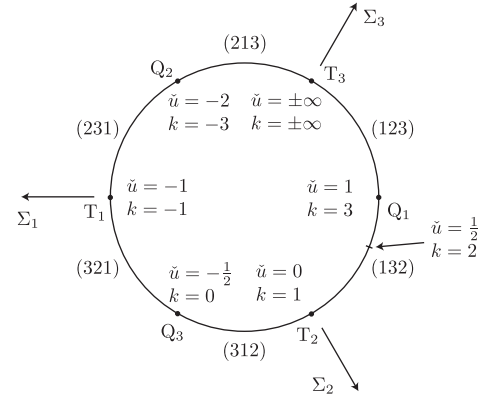$$p_1^2 + p_2^2 + p_3^2 = 1. \tag{13}$$



FIG. 1. The division of the Kasner circle $K^\circ$ of fixed points into six equivalent sectors and six LRS fixed points $T_\alpha$ and $Q_\alpha$, $\alpha = 1, 2, 3$. Sector $(\alpha\beta\gamma)$ is defined by $\Sigma_\alpha < \Sigma_\beta < \Sigma_\gamma$. The values of the extended Kasner parameter $\breve{u}$, cf. (17), along $K^\circ$ are indicated by the values of $\breve{u}$ at the LRS fixed points; in addition, $k = 2\breve{u} + 1$ is given.

Note that the integration constants on the local boundary are constants in time but functions of the spatial coordinates, in the $G_2$ case of $z$. For this reason the above Kasner exponents are called generalized exponents. The Kasner circle is divided into six equivalent sectors, which are associated with axes permutations and denoted by permutations of the triple (123): Sector $(\alpha\beta\gamma)$ is characterized by $p_\alpha < p_\beta < p_\gamma$, see Fig. 1. The boundaries of the sectors are six special points that are associated with locally rotationally symmetric (LRS) solutions,

$$T_\alpha: (\Sigma_\alpha, \Sigma_\beta, \Sigma_\gamma) = (+2, -1, -1) \quad \text{or, equivalently,} \quad (p_\alpha, p_\beta, p_\gamma) = (1, 0, 0) \tag{14a}$$

$$Q_\alpha: (\Sigma_\alpha, \Sigma_\beta, \Sigma_\gamma) = (-2, +1, +1) \quad \text{or, equivalently,} \quad (p_\alpha, p_\beta, p_\gamma) = \left(-\frac{1}{3}, \frac{2}{3}, \frac{2}{3}\right). \tag{14b}$$

The *Taub points* $T_\alpha$, $\alpha = 1, 2, 3$, correspond to the flat LRS solutions—the Taub representation of Minkowski spacetime, while $Q_\alpha$, $\alpha = 1, 2, 3$, are associated with three equivalent LRS solutions with nonflat geometry.

A frame independent (gauge invariant) way of representing the Kasner exponents $p_\alpha$ is by means of the (standard) Kasner parameter $u$; for each of the six equivalent sectors $(\alpha\beta\gamma)$ we have

$$p_\alpha = -u/f(u), \qquad p_\beta = (1 + u)/f(u),$$
$$p_\gamma = u(1 + u)/f(u), \tag{15}$$

where $u \in (1, \infty)$, while the boundary points of sector $(\alpha\beta\gamma)$, $Q_\alpha$ and $T_\gamma$, are characterized by $u = 1$ and $u = \infty$,

respectively. The function $f$, which will be used extensively, see also, e.g., Ref. [4] is defined by

$$f = f(x) := 1 + x + x^2. \tag{16}$$

In addition to the standard Kasner parameter $u$, we follow Ref. [20] and define the *extended* Kasner parameter $\breve{u}$ by

$$p_1 = -\breve{u}/f(\breve{u}), \qquad p_2 = (1 + \breve{u})/f(\breve{u}),$$
$$p_3 = \breve{u}(1 + \breve{u})/f(\breve{u}), \tag{17}$$

where $\breve{u} \in (-\infty, \infty)$ so that each value of $\breve{u}$ distinguishes a unique point on the Kasner circle; see Fig. 1. Comparing (15) and (17) we obtain a transformation between $u$ and $\breve{u}$ for each sector:

$$(123): (1, \infty) \ni \check{u} = u, \qquad (18a)$$

$$(312): \left(-\frac{1}{2}, 0\right) \ni \check{u} = -\frac{1}{u + 1}, \qquad (18b)$$

$$(231): \left(-2, -1\right) \ni \check{u} = -\frac{u + 1}{u}, \qquad (18c)$$

$$(132): (0, 1) \ni \check{u} = u^{-1}, \qquad (18a)$$

$$(321): \left(-1, -\frac{1}{2}\right) \ni \check{u} = \frac{u}{u + 1}, \qquad (18b)$$

$$(213): \left(-\infty, -2\right) \ni \check{u} = -(u + 1), \qquad (18c)$$

## B. Frame transitions

In the previous subsection the generalized Kasner metric is represented in a Fermi propagated frame with diagonalized shear (which is at the same time an Iwasawa frame). However, it is possible to represent the Kasner metric in a rotating spatial frame (e.g., a rotating Iwasawa frame), which leads to a time-dependent and nondiagonal Hubble-normalized shear. Since the frame invariants of the shear tensor, i.e., its trace, square, and determinant, must remain constants in time, the generalized Kasner metric in a (rotating) Iwasawa frame (for which $R_2 = 0$) is characterized by the relations

$$0 = \Sigma_1 + \Sigma_2 + \Sigma_3, \qquad (19a)$$

$$1 = \Sigma^2 = \frac{1}{6}(\Sigma_1^2 + \Sigma_2^2 + \Sigma_3^2) + \frac{1}{3}(R_1^2 + R_3^2), \qquad (19b)$$

$$\text{const} = \det\Sigma_{\alpha\beta} = \Sigma_1\Sigma_2\Sigma_3 - \Sigma_1 R_1^2 - \Sigma_3 R_3^2, \qquad (19c)$$

where the constant is merely a constant in time.

A frame rotation in the 2–3 plane corresponds to $R_1 \neq 0$, $R_3 = 0$, and thus, from (19c), by means of (19a) and (19b),

$$\Sigma_1(\Sigma_2\Sigma_3 - R_1^2) = \Sigma_1\left(\frac{1}{2}(\Sigma_2 + \Sigma_3)^2 + \frac{1}{2}\Sigma_1^2 - 3\right)$$

$$= \Sigma_1(\Sigma_1^2 - 3) = \text{const.} \qquad (20)$$

Since $\Sigma_1 = \text{const}$, this implies straight lines in $(\Sigma_1, \Sigma_2, \Sigma_3)$ space; see Fig. 2(a). A single straight line represents a Kasner solution (or a generalized Kasner metric corresponding to a constant value of $\check{u}$) in a frame that is rotating in the

2–3 plane. Analogously, for a frame rotation in the 1–2 plane we have $R_1 = 0$, $R_3 \neq 0$, and the straight lines $\Sigma_3 = \text{const}$; see Fig. 2(b). We refer to the trajectories that individual frame rotations give rise to as *single frame transitions*, $\mathcal{T}_{R_1}$ and $\mathcal{T}_{R_3}$. Double frame transitions $\mathcal{T}_{R_1 R_3}$, for which $R_1 R_3 \neq 0$, are not expected to play an essential role in the asymptotic dynamics of solutions toward a generic spacelike singularity; see Ref. [51], and we therefore refrain from a discussion (the interested reader is referred to Appendices B and C in Ref. [51]). Note that transitions (i.e., solution trajectories) are occasionally referred to as *orbits*. Note that the effect of a frame transition is to connect a Kasner state with the same Kasner state, but with an axes permutation.

Linearizing the equations for $R_1$ and $R_3$ in Appendix C at $\text{K}^\circ$ gives

$$-\partial_0 R_1|_{\text{K}^\circ} = (\Sigma_2 - \Sigma_3)|_{\text{K}^\circ} R_1 = 3(p_2 - p_3)R_1,$$
$$-\partial_0 R_3|_{\text{K}^\circ} = 3(p_1 - p_2)R_3. \qquad (21)$$

Hence the frame transitions $\mathcal{T}_{R_1}$ originate from sectors (321), (312), (132) and the points $Q_3$ and $T_2$, where $R_1$ is unstable (with respect to a time directed toward the past); see Fig. 2(a). We say that a frame transition $\mathcal{T}_{R_1}$ is *triggered* by $R_1$; similarly, $R_3$ triggers the frame transitions $\mathcal{T}_{R_3}$ in sectors (213), (231), (321) and at $Q_2$, $T_1$, see Fig. 2(b). Frame transitions map points of $\text{K}^\circ$ to each other; these maps can be expressed as the following maps of the extended Kasner parameter $\check{u}$:

$$\mathcal{T}_{R_1}: \check{u} \mapsto \check{u}^{-1}, \qquad \mathcal{T}_{R_3}: \check{u} \mapsto -(\check{u} + 1). \qquad (22)$$

## C. Curvature transitions

The Bianchi type II solutions on the local boundary are characterized by the vanishing of all variables except for the Hubble-normalized shear variables and the commutator function $N_1$. The simplest representation is with respect to a Fermi propagated frame in which the shear has been diagonalized (which is an Iwasawa frame at the same time), i.e., $R_\alpha = 0 \ \forall \ \alpha$. The Bianchi type II solutions can be conveniently parametrized as follows:

$$\Sigma_1 = -4 + (1 + \check{u}^2)\zeta, \qquad \Sigma_\beta = 2 - \check{u}^2\zeta,$$
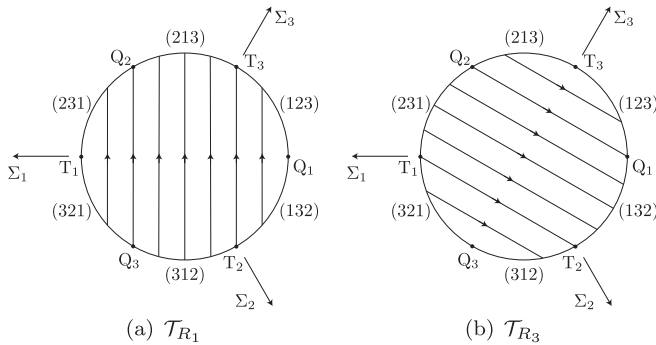$$\Sigma_\gamma = 2 - \zeta, \qquad (23)$$



FIG. 2. Projections of the two types of single frame transitions, $\mathcal{T}_{R_1}$ and $\mathcal{T}_{R_3}$, that exist in the $G_2$ case onto $(\Sigma_1, \Sigma_2, \Sigma_3)$ space. Throughout this paper, the direction of time, as indicated by the arrows, is toward the past.

where $\check{u} = \check{u}_- \in (0, +\infty)$ parametrizes the different possible initial Kasner states and $\zeta$ is monotonically increasing; see (26). In the projection onto $(\Sigma_1, \Sigma_2, \Sigma_3)$ space, (23) describes a family of straight lines originating from the point $(\Sigma_1, \Sigma_2, \Sigma_3) = (-4, 2, 2)$ outside of $K^\circ$; see Fig. 3. At the same time, the variable $N_1$ is determined by the constraint

$$\frac{1}{6}(\Sigma_1^2 + \Sigma_2^2 + \Sigma_3^2) + \frac{1}{12}N_1^2 = 1. \tag{24}$$

We refer to the type II trajectories as *single curvature transitions* $\mathcal{T}_{N_1}$, where each trajectory connects two different Fermi propagated Kasner states.

Linearizing the equation for $N_1$ in Appendix C at $K^\circ$ gives

$$-\partial_0 N_1|_{K^\circ} = -2(1 + \Sigma_1)|_{K^\circ} N_1 = -6p_1 N_1. \tag{25}$$

It follows that $N_1$ is unstable in sectors (123), (132) and at $Q_1$ toward the past, and accordingly we say that the curvature transitions $\mathcal{T}_{N_1}$ are "triggered" by $N_1$ on this part of $K^\circ$; see Fig. 3.

The function $\zeta$ in (23) is governed by the equation

$$\frac{\partial}{\partial(ut)}\zeta = 6|\check{u}_\pm|^{-1}\left(1 - \frac{\zeta}{\zeta_+}\right)\left(\frac{\zeta}{\zeta_-} - 1\right),$$
$$\text{where } \zeta_\pm = \frac{3}{f(\check{u}_\pm)}, \tag{26}$$

which has the solution

$$\zeta = \frac{3}{f(\check{u}_-)\frac{1-T}{2} + f(\check{u}_+)\frac{1+T}{2}} \text{ with } T := \tanh(2ut), \tag{27}$$

so that $\zeta$ is monotonically increasing from $\zeta_-$ to $\zeta_+$. By $u = u_-$ we denote the initial (standard) Kasner parameter; $\check{u}_\pm$ is the initial or final extended Kasner parameter. It follows from (23) that a single curvature transition $\mathcal{T}_{N_1}$ gives rise to a map

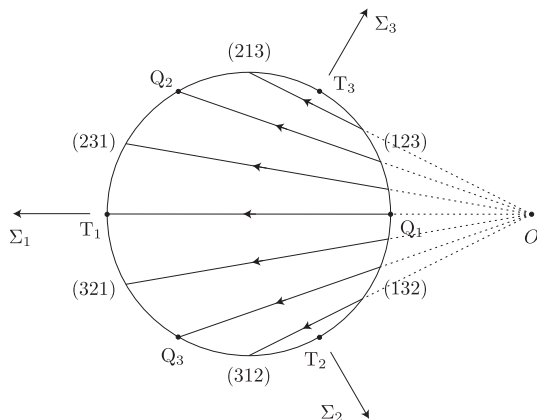$$\mathcal{T}_{N_1}: \check{u} = \check{u}_- \mapsto \check{u}_+ = -\check{u}_-. \tag{28}$$



FIG. 3. Projections onto $(\Sigma_1, \Sigma_2, \Sigma_3)$ space of the single curvature transitions $\mathcal{T}_{N_1}$.

In terms of the standard Kasner parameter $u$ this translates to $u_- \mapsto u_+ = u_- - 1$ if $u_- \geq 2$ and $u_- \mapsto u_+ = (u_- - 1)^{-1}$ if $1 \leq u_- < 2$, which is the usual representation of the Kasner map.

The Bianchi type II metric assumes a less transparent form in an Iwasawa frame that is rotating with respect to a Fermi propagated frame. In this case we speak of mixed curvature-frame transitions since $N_1 \neq 0$ and $R_1$ or $R_3 \neq 0$ simultaneously; see Appendix D in Ref. [51] for a discussion. Although the trajectory of a mixed curvature-frame transition looks rather complicated, the final state on $K^\circ$ coincides with the point obtained by successively applying the corresponding single curvature transition and the relevant single frame transition(s); single transitions thus act as building blocks that determine the final state of multiple transitions. In any case, just like double frame transitions, the mixed curvature-frame transitions are expected to not play a role in asymptotic dynamics of solutions toward a generic spacelike singularity; see Ref. [51].

### D. Spike transitions

Together with $K^\circ$ the frame and curvature transitions on the local boundary constitute the essential building blocks for the description of the asymptotic dynamics of $G_2$ models along "generic" time lines; see Secs. IV and V. Evidently, frame-curvature transitions and concatenations thereof concern the BKL scenario of (asymptotic) locality in which the dynamics of time lines decouple from their neighbors. However, to obtain a complete description of the dynamics of $G_2$ models toward generic spacelike singularities, the failure of asymptotic locality along particular time lines needs to be taken into account. This failure of locality is associated with the formation and recurrence of spikes; the central building block to describe this *nonlocal* scenario is the class of nonlocal transitions ("spike transitions") associated with the "explicit spike solutions" found by Lim [56].

The *explicit spike solutions* are $G_2$ OT vacuum solutions (i.e., $n_2 = n_3 = 0$) that in the area time gauge (3)–(5) take the form[3]

$$b^1 = \frac{1}{2}[-t - \log\text{sech}(wt)$$
$$+ \log(1 + (we^t z\text{sech}(wt))^2)], \tag{29a}$$
$$b^2 = t - b^1, \tag{29b}$$
$$b^3 = \frac{1}{4}[(3 + w^2)t + 4\log\text{sech}(wt)$$
$$- 2\log(1 + (we^t z\text{sech}(wt))^2)], \tag{29c}$$
$$n_1 = \frac{1}{2}w[e^{-2t} + 2(w\tanh(wt) - 1)z^2], \tag{29d}$$

[3]The solutions are presented here in a slightly different form than in Refs. [56,57]. Note also that, as stated in Ref. [57], there is a typographical error in equation (34) in Ref. [56]. For further discussion, see Sec. IV.

where $w > 0$. However, it is possible to let $w \in \mathbb{R}$, but $w \mapsto -w$ has the same effect as the coordinate reflection $y \mapsto -y$ and thus results in the same solution, cf. (40); in addition, the solution with $w = 0$ is trivial and not associated with a transition since it corresponds to the Kasner fixed point with $\check{u} = 1/2$.

In the following we analyze the explicit spike solutions (29) in terms of Hubble-normalized variables. For this purpose we define

$$T := \tanh(wt), \quad \vartheta(T) := (1-T)^{1-\frac{1}{w}}(1+T)^{1+\frac{1}{w}},$$
$$g_\pm(T,z) := 1 \pm \vartheta(T)w^2z^2. \tag{30}$$

The time variable $T$ is bounded; $t \in (-\infty, \infty)$ corresponds to $T \in (-1, 1)$. The limit $T \to \pm 1$ yields

$$\lim_{T \to -1} \vartheta(T) = 0, \quad \lim_{T \to +1} \vartheta(T) = \begin{cases} 0 & w > 1 \\ \infty & w < 1 \end{cases} \Rightarrow \tag{31a}$$
$$\lim_{T \to -1} g_\pm(T,z) = 1, \quad \lim_{\substack{T \to +1 \\ w > 1}} g_\pm(T,z) = 1,$$
$$\lim_{\substack{T \to +1 \\ w < 1}} g_\pm(T,z) = \begin{cases} 1 & z = 0 \\ \pm\infty & z \neq 0. \end{cases} \tag{31b}$$

Using the variable transformation given in Appendix B leads to

$$\tilde{p}_1 := \frac{1}{3}(1+\Sigma_1) = \frac{2w(T-\frac{1}{w})g_-(T,z)}{(w^2+3)g_+(T,z) - 4w(T-\frac{1}{w})}, \tag{32a}$$

$$\tilde{p}_2 := \frac{1}{3}(1+\Sigma_2) = \frac{4g_+(T,z) - 2w(T-\frac{1}{w})g_-(T,z)}{(w^2+3)g_+(T,z) - 4w(T-\frac{1}{w})}, \tag{32b}$$

$$\tilde{p}_3 := \frac{1}{3}(1+\Sigma_3) = \frac{(w^2-1)g_+(T,z) - 4w(T-\frac{1}{w})}{(w^2+3)g_+(T,z) - 4w(T-\frac{1}{w})}, \tag{32c}$$

where $\tilde{p}_1 + \tilde{p}_2 + \tilde{p}_3 = 1$, since $\Sigma_1 + \Sigma_2 + \Sigma_3 = 0$, and where

$$N_1 = 12w\frac{\sqrt{\vartheta(T)}z}{g_-(T,z)}\tilde{p}_1, \qquad N_{12} = \frac{1}{2}\frac{\sqrt{1-T^2}}{T-\frac{1}{w}}N_1,$$
$$R_3 = -3\frac{\sqrt{1-T^2}}{T-\frac{1}{w}}\tilde{p}_1. \tag{33}$$

From these expressions it is straightforward to describe the behavior of the explicit spike solutions (29). Henceforth, by explicit spike solution we typically mean its representation in Hubble-normalized variables and its projection onto $(\Sigma_1, \Sigma_2, \Sigma_3)$ space.

In contrast to frame and curvature transitions, an explicit spike solution consists of an entire family of curves parametrized by the spatial coordinate $z$. As $t \to -\infty$ ($T \to -1$), each spike solution (29) converges to a point on the Kasner circle $\mathrm{K}^\circ$ described by the extended Kasner parameter $\check{u} = \check{u}_- \in (1/2, +\infty)$, which we call the initial extended Kasner parameter, given by

$$\check{u} = \check{u}_- = \frac{1}{2}(w+1), \qquad (\Leftrightarrow w = 2\check{u} - 1). \tag{34}$$

This relation becomes manifest when we use an alternative form of (32) replacing $w$ by $2\check{u} - 1$, e.g.,

$$\tilde{p}_1 = \frac{-[\check{u}(\frac{1-T}{2}) + (1-\check{u})(\frac{1+T}{2})]g_-(T,z)}{f(\check{u})(\frac{1-T}{2}) + f(1-\check{u})(\frac{1+T}{2}) + f(\check{u}-1)\vartheta(T)w^2z^2}. \tag{32a}$$

Setting $T = -1$ and comparing with (17) establishes $\check{u}$ as the initial extended Kasner parameter according to (34). Note that the requirement $w > 0$ corresponds to $\check{u} > \frac{1}{2}$. If $\check{u} > 1$, it follows that the initial sector is (123), while if $\frac{1}{2} < \check{u} < 1$, the initial Kasner solution is in the part of sector (132) with $1 < u < 2$ [where we recall from (18) that $\check{u} = u$ if $\check{u} > 1$ and $\check{u} = u^{-1}$ if $0 < \check{u} < 1$].

In the limit $t \to \infty$ ($T \to 1$), however, a qualitative difference arises that leads to a classification of spike solutions in the OT $G_2$ context:

Hi A spike solution with $w > 1$ (i.e., $\check{u} = \check{u}_- > 1$) yields a *"high velocity"* spike transition, which we denote by $\mathcal{T}_{\text{Hi}}$. (The term velocity is defined in Appendix D). Its limit as $t \to -\infty$ ($T \to -1$) is a Kasner point in sector (123) with $\check{u} = \check{u}_- = (w+1)/2$, while its limit as $t \to \infty$ ($T \to 1$) is a Kasner point that belongs to one of the four sectors $(2\beta\gamma)$, $(3\beta\gamma)$. This final Kasner point for the spike solution is characterized by an extended Kasner parameter $\check{u}_+$. Letting $T \to 1$ in (32a′) shows that

$$\mathcal{T}_{\text{Hi}}: \check{u}_+ = 1 - \check{u}_-. \tag{35}$$

By means of (18), the map (35) can be expressed in terms of the standard frame-invariant Kasner parameter according to the map:

$$\mathcal{T}_{\text{Hi}}: u_+ = \begin{cases} u_- - 2 & u_- \in [3, \infty) \\ (u_- - 2)^{-1} & u_- \in [2, 3] \\ ((u_- - 1)^{-1} - 1)^{-1} & u_- \in [3/2, 2] \\ (u_- - 1)^{-1} - 1 & u_- \in [1, 3/2], \end{cases} \tag{35′}$$

where $u = u_-$ and $u_+$ are the initial and final Kasner parameters, respectively. We refer to Figs. 4(a) and 4(b) for a depiction of the projection of high velocity spike transitions onto $(\Sigma_1, \Sigma_2, \Sigma_3)$ space.

Lo A spike solution with $0 < w < 1$ (i.e., $\frac{1}{2} < \check{u} = \check{u}_- < 1$) yields a *"low velocity'''* spike solution, which we denote by $\mathcal{S}_{\text{Lo}}$. Its limit as $t \to -\infty$ ($T \to -1$) is a Kasner point in the part of sector (132) with $\check{u} > \frac{1}{2}$ ($u < 2$), which yields $u = u_- = 2/(w+1)$ since $u = \check{u}^{-1}$. Its limit as $t \to \infty$ ($T \to 1$) is a generalized Kasner metric with a discontinuous Kasner parameter which is because the limit of $g_+(T,z)$ as $T \to 1$ is discontinuous, cf. (31b). From (32a′) it follows that

$$\mathcal{S}_{\text{Lo}}: \check{u}_+(z) = \begin{cases} 1 - \check{u}_- & z = 0 \\ \check{u}_- - 1 & z \neq 0, \end{cases} \tag{36}$$

which in terms of the standard Kasner parameter results in

$$\mathcal{S}_{\text{Lo}}: u_+(z) = \begin{cases} u_-(u_- - 1)^{-1} & z = 0 \\ (u_- - 1)^{-1} & z \neq 0. \end{cases} \tag{36′}$$
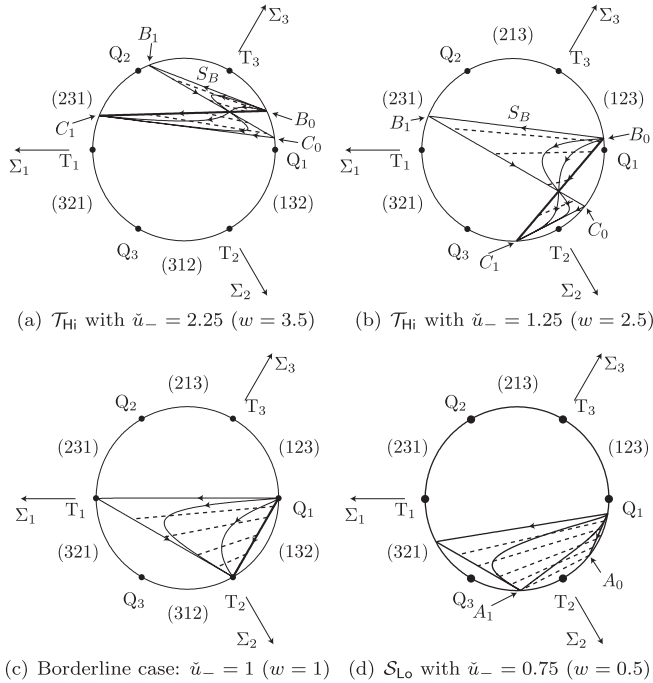
(a) $\mathcal{T}_{\mathsf{Hi}}$ with $\check{u}_- = 2.25$ $(w = 3.5)$

(b) $\mathcal{T}_{\mathsf{Hi}}$ with $\check{u}_- = 1.25$ $(w = 2.5)$

(c) Borderline case: $\check{u}_- = 1$ $(w = 1)$

(d) $\mathcal{S}_{\mathsf{Lo}}$ with $\check{u}_- = 0.75$ $(w = 0.5)$

FIG. 4. High velocity spike transitions $\mathcal{T}_{\mathsf{Hi}}$ and low velocity spike solutions $\mathcal{S}_{\mathsf{Lo}}$ projected onto $(\Sigma_1, \Sigma_2, \Sigma_3)$ space. Each $\mathcal{T}_{\mathsf{Hi}}$ or $\mathcal{S}_{\mathsf{Lo}}$ corresponds to a family of curves parametrized by the spatial coordinate $z$. The thick (straight) lines represent the trajectories of the time lines of the spike surface $z = 0$, i.e., spike surface trajectories $\mathcal{T}_S$. The thin curves represent the trajectories of time lines $0 \neq |z| \ggg 1$. The thin straight lines represent $|z| \gg 1$ time lines; these are short BKL chains, i.e., sequences of curvature-frame transitions. The dashed lines represent constant time slices of a solution.

Therefore the limit (as $t \to \infty$) of the low velocity spike solution along the time lines of the spike surface $z = 0$ differs from the limit along the other time lines. The trajectory in $(\Sigma_1, \Sigma_2, \Sigma_3)$ space representing the spike surface ends in the part of sector (132) with $u > 2$ $(0 < \check{u} < \frac{1}{2})$, while trajectories associated with time lines with $z \neq 0$ meet in a point of sector (312); see Figs. 4(d) and 5. This behavior of the low velocity spike solution results in the convergence of, e.g., the Hubble-normalized Kretschmann scalar to a discontinuous limit.

The trajectories of an explicit spike solution that represent time lines with $|z| \gg 1$ (i.e., time lines far from the spike surface $z = 0$) are approximated by a succession of (two or three) curvature-frame transitions; see Fig. 4. (In Secs. IV and V we will refer to finite and infinite sequences of curvature-frame transitions as *BKL chains*.) In the case of a high velocity spike transition $\mathcal{T}_{\mathsf{Hi}}$, trajectories with $|z| \gg 1$ are approximated by the chain $\mathcal{T}_{N_1}$-$\mathcal{T}_{R_3}$-$\mathcal{T}_{N_1}$; in the case of a low velocity spike solution $\mathcal{S}_{\mathsf{Lo}}$, $|z| \gg 1$ trajectories are approximated by a $\mathcal{T}_{N_1}$ transition followed by a $\mathcal{T}_{R_3}$ transition. Formally, these chains are the limit as $z \to \pm\infty$ of the orbits representing a spike solution. Since
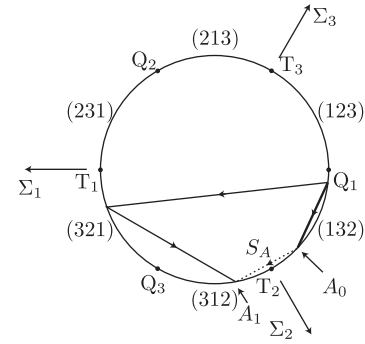


FIG. 5. The "skeleton" of a $\mathcal{S}_{\mathsf{Lo}}$ spike solution described by the spike surface trajectory $\mathcal{T}_S$ (thick line) and the short BKL chain representing the trajectories associated with $|z| \gg 1$, cf. Fig. 4; in addition the dashed line $S_A$ corresponds to a "missing" curvature transition $\mathcal{T}_{N_1}$ that would reunite the spike surface $z = 0$ with the $z \neq 0$ trajectories.

$\mathcal{T}_{N_1}$ is associated with the map $\check{u} \mapsto -\check{u}$ while $\mathcal{T}_{R_3}$ gives $\check{u} \mapsto -(\check{u} + 1)$, it follows that

$$\mathsf{Hi}: \check{u}_- \overset{\mathcal{T}_{N_1}}{\mapsto} -\check{u}_- \overset{\mathcal{T}_{R_3}}{\mapsto} -(-\check{u}_- + 1) \overset{\mathcal{T}_{N_1}}{\mapsto} 1 - \check{u}_- = \check{u}_+$$

(37)

in the high velocity case, which coincides with (35). In the low velocity case the final $\mathcal{T}_{N_1}$ transition is missing so that

$$\mathsf{Lo}: \check{u}_- \overset{\mathcal{T}_{N_1}}{\mapsto} -\check{u}_- \overset{\mathcal{T}_{R_3}}{\mapsto} -(-\check{u}_- + 1) = \check{u}_- - 1 = \check{u}_+, \quad (38)$$

which coincides with the $z \neq 0$ case of (36).

The evolution of the Hubble-normalized variables along the time lines of the spike surface $z = 0$ itself is represented by a single straight line in $(\Sigma_1, \Sigma_2, \Sigma_3)$ space, which we refer to as the *spike surface trajectory* $\mathcal{T}_S$. The family of "spike surface trajectories" (parametrized by $w$ or $\check{u}_-$) has a common focal point: Each spike surface trajectory $\mathcal{T}_S$ corresponds to a straight line that originates from the point $(\Sigma_1, \Sigma_2, \Sigma_3) = (-\frac{5}{2}, \frac{1}{2}, 2)$ outside $\mathrm{K}^{\circ}$; see Fig. 6. In the high velocity case, the spike surface trajectories enter the physical state space in sector (123), while in the low velocity case, they enter the physical state space in the
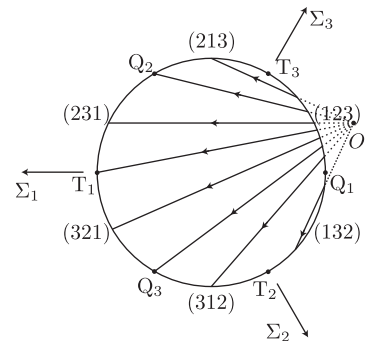


FIG. 6. Projections of spike surface trajectories $\mathcal{T}_S$ onto $(\Sigma_1, \Sigma_2, \Sigma_3)$ space.

part of sector (132) with $1 < u < 2$, i.e., $\frac{1}{2} < \check{u} < 1$. From (32) we see that

$$\Sigma_1|_{z=0} = -\frac{5}{2} + \frac{1}{2}f(-\check{u}_\pm)\chi,$$

$$\Sigma_2|_{z=0} = \frac{1}{2} + \chi - \frac{1}{2}f(-\check{u}_\pm)\chi, \qquad (39a)$$

$$\Sigma_3|_{z=0} = 2 - \chi,$$

where

$$\chi = \frac{3}{f(\check{u}_-)\frac{1-T}{2} + f(\check{u}_+)\frac{1+T}{2}}, \qquad (39b)$$

so that $\chi$ increases monotonically from $\chi_- = 3/f(\check{u}_-)$ to $\chi_+ = 3/f(\check{u}_+)$. The expression $f(-\check{u}_\pm)$ appearing in (39a) stands for $f(-\check{u}_-)$ or $f(-\check{u}_+)$; either can be used since they coincide.

Finally, the trajectories representing time lines $z \neq 0$ that are not far from the spike surface "interpolate" between the two types of behavior, i.e., $|z| \gg 1$ and $z = 0$, described previously. This family of trajectories is rather complicated, see Fig. 4 and Ref. [56]; we note, however, that all trajectories intersect at $T = 1/w$ in $(\Sigma_1, \Sigma_2, \Sigma_3)$ space, as follows from (32).

In Eq. (29) we have presented the principal form of the explicit spike solution. There exist, however, entire families of explicit spike solutions with different *coordinate widths* and *time offsets*. These spike solutions are required when spikes are concatenated, i.e., joined with each other in chains, which we discuss in Secs. IV and V. We therefore consider the constant coordinate transformation $(x, y, z) \mapsto (\bar{x}, \bar{y}, \bar{z})$ given by $x = c^1{}_1\bar{x} + c^1{}_2\bar{y}$, $y = c^2{}_2\bar{y}$, and $z = c^3{}_3\bar{z}$; in addition we may consider a rescaling of time, i.e., $t \mapsto \bar{t}$ with $t = c^0{}_0\bar{t}$. This coordinate transformation preserves the form (45) of the metric provided that $c^0{}_0 = |c^1{}_1 c^2{}_2 c^3{}_3|$ and induces the transformation $(b^1, b^2, b^3, n_1) \mapsto (\bar{b}^1, \bar{b}^2, \bar{b}^3, \bar{n}_1)$ with

$$\bar{b}^1 = b^1 - \log|c^1{}_1|, \qquad \bar{b}^2 = b^2 - \log|c^2{}_2|,$$

$$\bar{b}^3 = b^3 - \log|c^3{}_3|, \qquad \bar{n}_1 = \frac{c^1{}_2}{c^1{}_1} + \frac{c^2{}_2}{c^1{}_1}n_1. \qquad (40)$$

Choosing $c^1{}_1 = (2Q_0)^{-1/2}$, $c^1{}_2 = (2Q_0)^{-1/2}Q_2$, $c^2{}_2 = (2Q_0)^{1/2}$, and $c^3{}_3 = \exp(-\lambda_2/4)$ reproduces the free constants $Q_0$, $Q_2$, and $\lambda_2$ of Eqs. (33)–(35) in Ref. [56] and Eqs. (A3)–(A5) in Ref. [57]; note, however, that $\{c^1{}_1, c^1{}_2, c^2{}_2, c^3{}_3\}$ are four free constants. Restricting ourselves to the case $c^0{}_0 = 1$ (so that $|c^1{}_1 c^2{}_2 c^3{}_3| = 1$) it follows from conceptual considerations or directly from the relations of this section and Appendix B that the Hubble scalar and the Hubble-normalized variables are unaffected by (40), although the frame variable $E_3$, transforms like $E_3 \mapsto \bar{E}_3 = (c^3{}_3)^{-1}E_3$. As a consequence, Eqs. (32) and (33) take the same form, where $z \mapsto c_z z$, $c_z := c^3{}_3$, so that, e.g.,

$$g_\pm(T, z) = 1 \pm \vartheta(T)w^2 c_z^2 z^2. \qquad (41)$$

Equation (29) with $z \mapsto c_z z$ yields a family of spike solutions and transitions with different coordinate widths, an inverse measure of which is, e.g., the constant $c_z$. It follows from (33) that

$$c_z = (12w\sqrt{\vartheta(T)}\tilde{p}_1|_{z=0})^{-1}\partial_z N_1|_{z=0}. \qquad (42a)$$

To eliminate $T$ we make use of the trajectory of the spike surface $z = 0$, because this trajectory is not affected by the spike width; using $\tilde{p}_1|_{z=0}$, see (32a), we obtain

$$\vartheta(T) = \frac{4}{w^2(1 + 2\tilde{p}_1|_{z=0})^2}(-\check{u}_+ - f(\check{u}_+)\tilde{p}_1|_{z=0})^{1-\frac{1}{w}}$$

$$\times (\check{u}_- + f(\check{u}_-)\tilde{p}_1|_{z=0})^{1+\frac{1}{w}}, \qquad (42b)$$

where $\check{u}_-$ ($\check{u}_+$) is the initial (final) point of $\mathcal{T}_{\mathsf{Hi}}$ or $\mathcal{S}_{\mathsf{Lo}}$ (for $z = 0$), i.e., $\check{u}_+ = 1 - \check{u}_-$, $w = 2\check{u}_- - 1$. Inserting (42b) into (42a) we obtain an explicit formula for $c_z$ in terms of certain Hubble-normalized variables (and a spatial derivative).

While a rescaling of the spatial coordinate $z$ yields a spike solution with a different coordinate width, a translation in $z$ puts the spike surface at a different spatial location. Analogously, translations in time ("time offsets"), i.e., $t \mapsto t \pm t_0$, yield spike solutions with a different temporal flow (which, of course, does not affect the orbits in the diagrams). In this case, the "time" $T$ of (30) is redefined as $T = \tanh[w(t \pm t_0)]$.

### E. Bill **spiky features**

High velocity spike transitions $\mathcal{T}_{\mathsf{Hi}}$ originate from Kasner points with $1 < \check{u} < \infty$, i.e., from sector (123), low velocity spike solutions $\mathcal{S}_{\mathsf{Lo}}$ from points with $\frac{1}{2} < \check{u} < 1$, which covers merely the upper part of sector (132). The third type of spiky feature, which we call a Bill spiky feature, fills the rest of sector (132):

Bill The limit of a Bill spiky feature as $t \to -\infty$ is a Kasner point on sector (132) with $0 < \check{u} < \frac{1}{2}$, i.e., $u > 2$. The trajectories $z \neq 0$ of a Bill spiky feature coincide with the $\mathcal{T}_{N_1}$ transition that originate from the Kasner point $\check{u}$ on sector (132) and end in sector (312), while the spatial points of the spike surface $z = 0$ are left behind at the Kasner point $\check{u}$ on sector (132). Accordingly, the limit as $t \to \infty$ is a generalized Kasner metric with discontinuous Kasner parameter such that

$$\check{u}_+(z) = \begin{cases} \check{u}_- & z = 0 \\ -\check{u}_- & z \neq 0. \end{cases} \qquad (43)$$

In terms of the standard Kasner parameter we have $u_- \mapsto u_+ = u_-$ and $u_+ = u_- - 1$, respectively.

A Bill spiky feature is intimately connected with the "second half" of a low velocity spike solution $\mathcal{S}_{\mathsf{Lo}}$ in the neighborhood of $z = 0$. Specifically, consider a $\mathcal{S}_{\mathsf{Lo}}$ characterized by $w = 1 - 2\check{u}$ with $\check{u} \in (0, \frac{1}{2})$, (inverse)

coordinate spike width $c_z$, and a time offset $t_0$, i.e., $t$ is replaced by $t + t_0$ in (29). For a given value of $z = \tilde{z} \neq 0$, if $c_z$ is sufficiently small, the trajectory of $\tilde{z}$ will resemble the concatenation of the low velocity spike surface trajectory $\mathcal{T}_S$ and a $\mathcal{T}_{N_1}$ transition originating from $\breve{u}$. It is possible to choose a (large) value of $t_0$, which is fine-tuned with respect to $c_z$, such that the point $t = 0$ of the trajectory is close to the midpoint of the $\mathcal{T}_{N_1}$ transition. This motivates taking the combined limit $c_z \rightarrow 0$ and $t_0 \rightarrow \infty$ such that $2c_z e^{(1-w)t_0} = 1$, which, via (32), yields

$$\tilde{p}_1 = \frac{1}{3}(1 + \Sigma_1) = \frac{-\breve{u}(1 - (1 - 2\breve{u})^2 z^2 e^{4\breve{u}t})}{f(\breve{u}) + f(-\breve{u})(1 - 2\breve{u})^2 z^2 e^{4\breve{u}t}}, \quad (44a)$$

$$\tilde{p}_2 = \frac{1}{3}(1 + \Sigma_2) = \frac{2 - (1 - \breve{u})(1 - (1 - 2\breve{u})^2 z^2 e^{4\breve{u}t})}{f(\breve{u}) + f(-\breve{u})(1 - 2\breve{u})^2 z^2 e^{4\breve{u}t}}, \quad (44b)$$

$$N_1 = \frac{-12\breve{u}(1 - 2\breve{u})z e^{2\breve{u}t}}{f(\breve{u}) + f(-\breve{u})(1 - 2\breve{u})^2 z^2 e^{4\breve{u}t}}, \quad (44c)$$

while $R_3$ and $N_{12}$ are zero. The above expression is not a solution to Einstein's equations, but it is an inhomogeneous solution of the equations on the local boundary.

## IV. ASYMPTOTICS AND CONCATENATION IN THE OT CASE

In the present section we restrict our attention to the OT subclass of the $G_2$ models, of which the $T^3$ Gowdy models are a prominent special case; see Appendix A. The metric of the OT $G_2$ models is of the form (1), where $n_2 = n_3 = 0$, i.e.,

$$ds^2 = -N^2(dx^0)^2 + e^{-2b^1}(dx + n_1 dy)^2$$
$$+ e^{-2b^2}dy^2 + e^{-2b^3}dz^2, \quad (45)$$

where $b^\alpha = b^\alpha(x^0, z) \; \forall \alpha$ and $n_1 = n_1(x^0, z)$. The area time gauge entails $x^0 = t = b^1 + b^2$ (modulo a constant) and $N = -\sqrt{\det^{(3)}g}$. Recall from Sec. II that the conformally Hubble-normalized rotation variable $R_1$ vanishes identically under the OT assumption.

### A. BKL concatenation in OT compatible Bianchi models

Let us briefly recapitulate the basic facts about *spatially homogeneous* models in the present context. The existence of two commuting Killing vector fields is incompatible with the defining properties of the Bianchi type VIII and IX models. The Bianchi types that are compatible are types VII$_h$ and VI$_h$, and the "lower types," which can be obtained by means of Lie contractions. However, it is only the symmetry adapted frames of Bianchi types VII$_0$, VI$_0$, II, and I that are compatible with a line element (45) in the area time gauge; cf. Ref. [64].

The initial singularity of the spatially homogeneous OT $G_2$ vacuum models is known to be a Kasner-type singularity, i.e., the asymptotic behavior is that of a Kasner solution. This can be understood in connection
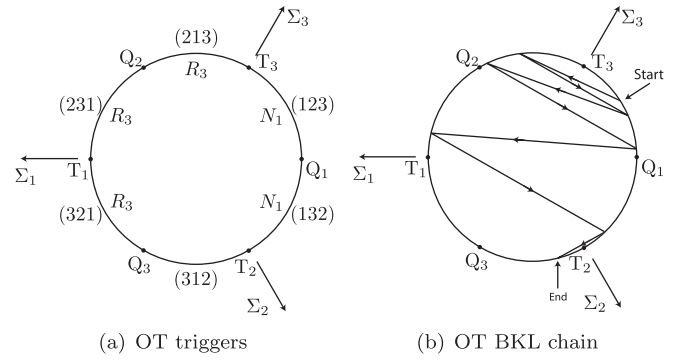


(a) OT triggers      (b) OT BKL chain

FIG. 7. In the OT case each sector is associated with a "trigger" ($N_1$ or $R_3$) except for sector (312) at which these variables are stable. As a consequence, OT BKL chains (i.e., concatenations of $\mathcal{T}_{N_1}$ and $\mathcal{T}_{R_3}$ transitions) are finite and terminate at sector (312).

with Fig. 7. For Bianchi models of type VI$_0$ and VII$_0$, in a non-Fermi frame, it follows from (21) and Fig. 2(b), and (25) and Fig. 3, respectively, that $R_3$ is an unstable variable triggered in three sectors of the Kasner circle while $N_1$ is triggered in two sectors; see Fig. 7(a). Sector (312), however, is a stable sector, which means that $N_1$ and $R_3$ are stable variables, i.e., a solution with initial data close to a Kasner point of sector (312) must converge to a Kasner point of that sector, because $N_1$ and $R_3$ decay exponentially. It is thus intuitive (and straightforward to prove, see, e.g., Ref. [51]) that every type VI$_0$ or type VII$_0$ model converges to a fixed point on the stable sector.

Considering Figs. 2(b) and 3 together, it is clear that frame transitions and curvature transitions can be concatenated (joined to form chains) by identifying the "final" fixed point ($\omega$-limit point) of one transition with the "initial" fixed point ($\alpha$-limit point) of another transition; see Fig. 7(b). Concatenation of $\mathcal{T}_{R_3}$ and $\mathcal{T}_{N_1}$ transitions yields finite heteroclinic chains,[4] which we refer to as OT *BKL chains*; these chains terminate on the stable sector (312).

The relevance of the OT BKL chains is immediate: The evolution of initial data sufficiently close to a Kasner point of any other than the stable sector (or, the evolution of data sufficiently close to a transition) is approximately described by an OT BKL chain, which yields a finite number of "oscillations" between Kasner states, mediated by $\mathcal{T}_{N_1}$ and $\mathcal{T}_{R_3}$ transitions, and convergence to a Kasner point on the stable sector (312). However, it should be pointed out that the evolution of initial data far from the Bianchi type I and the type II subsets (i.e., far from the Kasner circle and the transition orbits) need not bear any relation to OT BKL

---

[4]A heteroclinic orbit is an orbit (i.e. solution trajectory) that starts ($\alpha$-limit) and ends ($\omega$-limit) at two different fixed points. A heteroclinic chain is a sequence of heteroclinic orbits such that the $\omega$-limit point of one orbit is the $\alpha$-limit point of the subsequent orbit.

chains, although there is still convergence to a Kasner point on the stable sector. For a comprehensive study of type $VI_0$ or $VII_0$ dynamics (in a Fermi frame) we refer to Refs. [43,69] and references therein.

## B. Asymptotics of spatially inhomogeneous OT models

According to the BKL conjecture, asymptotic locality means that in the *inhomogeneous* case there exists a generic set of time lines whose evolution is governed asymptotically by the flow on the local boundary (which entails that the evolution of a single time line is congruent with the evolution of a spatially homogeneous model.) This does *not* mean, however, that the dynamics of spatially homogeneous models is sufficient to describe the dynamics of inhomogeneous models. On the contrary, spatially inhomogeneous OT models behave quite delicately in general.

However, Fig. 7(a) suggests a straightforward behavior for at least certain classes of initial data. Consider, e.g., initial data that constitute a small perturbation of a generalized Kasner metric associated with the stable sector (312) on $K^\bigcirc$, i.e., $\Sigma_1, \Sigma_2, \Sigma_3$ are functions of the spatial variable $z$ with values close to sector (312), while the remaining variables and the Hubble-normalized spatial frame derivatives are small; note that we do not exclude that, e.g., $N_1$ has zeros. Since neither $N_1$ nor $R_3$ are triggered but decay exponentially, we expect convergence to a generalized Kasner solution on sector (312). This is an asymptotic state that is often termed "asymptotically velocity dominated"; we refer to Appendix A, where we discuss results that turn the intuitive picture into a rigorous one in the case of $T^3$ Gowdy models.

Prescribing 'almost Kasner' initial data close to sector (321), on the other hand, leads to an exponential decay of $N_1$, while $R_3$ is triggered, so that an (approximate) $\mathcal{T}_{R_3}$ frame transition ensues at each spatial point,[5] which in turn leads to the convergence of the solution to a generalized Kasner metric of sector (312), as before.

Likewise, initial data close to sectors (231) or (213) lead to an initial frame transition $\mathcal{T}_{R_3}$, which takes the solution to sectors (132) or (123) where $N_1$ is the trigger. If $|N_1| > 0$ (in the optimal case: uniformly) we are led to expect the familiar behavior of the spatially homogeneous case, i.e., a subsequent (approximate) $\mathcal{T}_{N_1}$ curvature transition at each spatial point; accordingly, each time line follows an (approximate) OT BKL chain. On the other hand, if $N_1$ has zeros for certain values of the spatial coordinate $z$, the simple picture inspired by spatially homogeneous dynamics fails. At these spatial surfaces $N_1$ cannot drive the

---

[5]Technical difficulties occur if $R_3$ is zero initially at some value of $z$; in this case a false spike ensues. We refrain from discussing this case since it is a gauge effect (a "nuisance" as stated in Ref. [70]) and focus on true spatial structures instead. We note however that a complete description of a generic singularity in an Iwasawa frame necessarily involves gauge features of this kind.

further evolution of the solution. Instead, spatial structures (spikes) develop (which are true spikes in the sense of being gauge invariant features). In sectors (123) and (132) with $u > 2$, spatial gradients take the role of triggers at these special values of $z$ (and their neighborhoods) and spikes are formed that are approximately described by the explicit spike solutions, $\mathcal{T}_{Hi}$ for sector (123) and $\mathcal{S}_{Lo}$ for sector (132) when $u < 2$. In these cases the time lines associated with a zero in $N_1$ evolves according to a spike surface trajectory $\mathcal{T}_S$. This is in contrast to if a solution approaches sector (132) with $u > 2$; in this case a Bill spiky feature ensues and hence the evolution along the time lines associated with a zero in $N_1$ gets stuck at this sector while the evolution of the other time lines end at sector (312). This is further discussed in Sec. IV C.

We emphasize that the evolution of general initial data is rather complicated (and the heuristic considerations fail). However, asymptotic velocity dominance remains true in general, i.e., solutions converge to a generalized Kasner metric (which is in general associated with a discontinuous Kasner parameter); see Appendix A.

## C. Spike concatenation in OT models

In Sec. IV A we have concatenated curvature transitions and frame transitions to build OT BKL chains. The concept of concatenation in the context of finite dimensional dynamical systems is rigorously captured by the well-established concept of heteroclinic chains, which in the present context means matching of heteroclinic orbits at Kasner fixed points. Since the local boundary is effectively a finite dimensional system, although it really is an infinite set of copies of the same dynamical system, one copy for each spatial point, this concept is still valid. However, a solution on the local boundary may be described by several heteroclinic chains describing different evolution along different time lines. When it comes to the spike solutions each solution can be viewed as describing the evolution along a $z$-parametrized family of time lines, which complicates the issue of concatenation (joining solutions to each other based on their asymptotic properties toward the past and future). However, in the case that the evolution along *all* time lines of a solution share an asymptotic limit, in the present case a Kasner fixed point, then one can proceed in the same manner as when concatenating heteroclinic orbits to heteroclinic chains and match solutions to each other at these Kasner points, thus yielding a concatenated chain of solutions. High velocity spike transitions $\mathcal{T}_{Hi}$ and individual frame transitions $\mathcal{T}_{R_3}$ have this feature and can therefore be concatenated by identifying the final Kasner point of one transition with the initial Kasner point of another transition; see Figs. 8(a) and 8(b) Note that this is possible because the entire family of curves representing a $\mathcal{T}_{Hi}$ transition converges to a point on $K^\bigcirc$ as $t \to -\infty$ and to another point on $K^\bigcirc$ as $t \to \infty$. Concatenation of high velocity spike transitions $\mathcal{T}_{Hi}$ and

(a) $\mathcal{T}_{\mathsf{Hi}}-\mathcal{T}_{R_3}-\mathcal{T}_{\mathsf{Hi}}-\mathcal{T}_{R_3}$



(b) $\mathcal{T}_{\mathsf{Hi}}-\mathcal{T}_{R_3}-\mathcal{T}_{\mathsf{Hi}}$



(c) $\mathcal{T}_{\mathsf{Hi}}-\mathcal{T}_{R_3}-\mathcal{S}_{\mathsf{Lo}}$



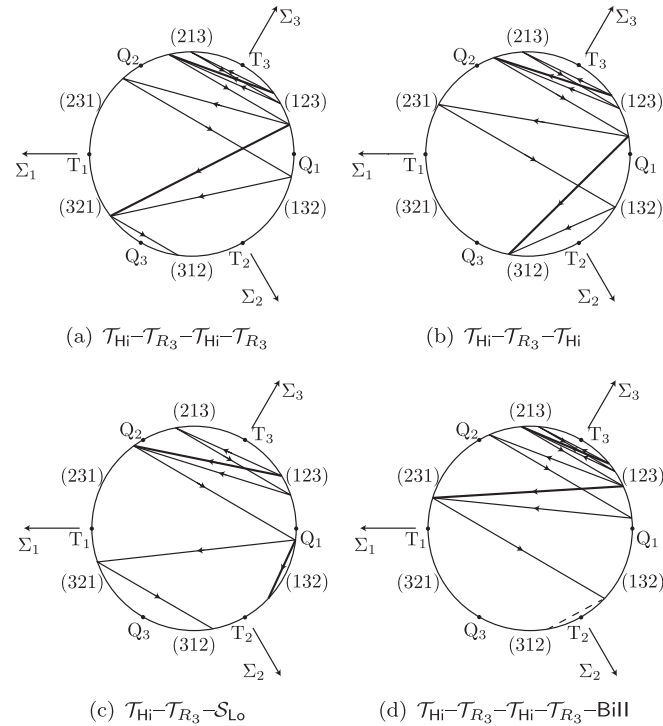(d) $\mathcal{T}_{\mathsf{Hi}}-\mathcal{T}_{R_3}-\mathcal{T}_{\mathsf{Hi}}-\mathcal{T}_{R_3}-\mathsf{Bill}$

FIG. 8. OT spike chains in the projection onto $(\Sigma_1, \Sigma_2, \Sigma_3)$ space; depicted are chains of the spike surface trajectories ($z = 0$) and trajectories associated with $|z| \gg 1$ (which are OT BKL chains). An OT spike chain is a high velocity chain (i.e., a concatenation of $\mathcal{T}_{\mathsf{Hi}}$ transitions and $\mathcal{T}_{R_3}$ frame transitions) ending with a $\mathcal{T}_{R_3}$ transition (a) or a $\mathcal{T}_{\mathsf{Hi}}$ transition (b); or there is one additional (final) transition: a low velocity solution $\mathcal{S}_{\mathsf{Lo}}$ (c) or a Bill spiky feature (d). The latter is depicted by a dashed line.

individual frame transitions $\mathcal{T}_{R_3}$ toward the past singularity yields finite chains, which we refer to as *high velocity chains*, however, concatenation in the opposite direction of the time coordinate, i.e., away from the singularity, yields infinite high velocity chains that converge to the Taub point $T_3$.

Tracking the extended Kasner parameter along a high velocity chain we find an alternation between the $\mathcal{T}_{\mathsf{Hi}}$ law $\check{u} \mapsto 1 - \check{u}$ and the $\mathcal{T}_{R_3}$ law $\check{u} \mapsto -(\check{u} + 1)$, whose combination results in $\check{u} \mapsto \check{u} - 2$. A high velocity chain either ends at a point on the stable Kasner sector (312), where the final transition can be a $\mathcal{T}_{R_3}$ as in Fig. 8(a) or a $\mathcal{T}_{\mathsf{Hi}}$ as in Fig. 8(b), or the chain ends at a point on sector (132). The latter case is particularly interesting, since the high velocity chain can then be continued by a $\mathcal{S}_{\mathsf{Lo}}$ solution or a Bill spiky feature, depending on its location in sector (132). We use the term *OT spike chains* as an umbrella term for the two cases; i.e., an OT spike chain is either a high velocity chain ending in sector (312) or a high velocity chain followed by a $\mathcal{S}_{\mathsf{Lo}}$ solution or a Bill spiky feature. Note that the continuation of OT spike chains beyond this point is impossible (because $\mathcal{T}_{R_1}$ transitions do not exist in the OT context; see, however, the next section). Note that for an OT spike chain ending with a $\mathcal{S}_{\mathsf{Lo}}$ solution
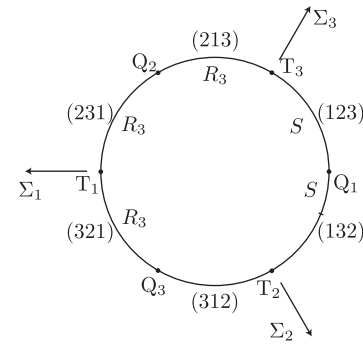


FIG. 9. Triggers for the evolution of the spike surface $z = 0$ in the OT case. In sectors (213), (231), and (321), $R_3$ triggers frame transitions $\mathcal{T}_{R_3}$. Since $N_1 = 0$ at $z = 0$, $N_1$ does not exist as a trigger; instead spatial gradients ($S$) take the role as triggers and lead to a spike surface trajectory $\mathcal{T}_S$; see Fig. 6. These triggers cover sectors (312) and (132) with $u > 2$. Sector (312) and sector (132) with $u < 2$ are stable in this context.

or a Bill spiky feature the trajectories of the points on the spike surface $z = 0$ end at sector (132) with $0 < \check{u} < 1/2$, while points with $z \neq 0$ are transported to the stable sector (312). Therefore, in a vague sense, the part of sector (132) with $0 < \check{u} < 1/2$ is "stable" for the spike surface; see Fig. 9.

The role of OT BKL chains for the OT class of spatially homogeneous models has been discussed in section IV A. Numerical evidence [57] suggests that OT spike chains fill the same function for inhomogeneous solutions with spikes. In the following we give a detailed description. For simplicity, we restrict our attention to *symmetric* initial data sets, by which we mean initial data such that $\Sigma_1$, $\Sigma_2$, $\Sigma_3$, and $R_3$ are even functions in $z$, while $N_1$ and $N_{12}$ are odd functions. We are interested in the nondegenerate case for which the gradients at $z = 0$ are nonvanishing and we also assume the "genericity condition" that $R_3 \neq 0$ at the spike surface $z = 0$. This type of initial data fixes the location of the spike surface at $z = 0$.[6] Note that the explicit spike solutions $\mathcal{T}_{\mathsf{Hi}}$, $\mathcal{S}_{\mathsf{Lo}}$, and the Bill spiky feature, see (32) and (44), respectively, are of this symmetric type. Since the location of the spike surface is fixed, it is simple to calculate the particle horizons associated with the spike world sheet $z = 0$. Since a null vector orthogonal to the surfaces of symmetry is of the form $(1, 0, 0, \pm e^{-t})^{\mathrm{T}}$, see (45), the particle horizon at $t$ of the $z = 0$ time lines is $[-e^{-t}, e^{-t}]$ times the symmetry surfaces; in particular, the particle horizons are shrinking rapidly (in $z$ direction) as $t \to \infty$. Hence the dynamics of a solution in a neighborhood of the spike world sheet for $t \geq t_0$ is completely determined by the initial data of the solution in a

---

[6]In general, this type of initial data fixes the location of *a* spike surface at $z = 0$. During the evolution of the data, it is possible that other (in general "moving") spikes form at different values of $z$. We refer to the concluding remarks.

neighborhood of $[-e^{-t_0}, e^{-t_0}]$. In particular, changing the initial data for an explicit spike solution outside a neighborhood of $[-e^{-t_0}, e^{-t_0}]$ does not affect the evolution (29) of the spike surface and its immediate neighbors. The asymptotic dynamics is thus local in the sense that *global topological aspects are irrelevant* once the particle horizon scale has become sufficiently small compared to the "global scale" associated with the topology. In the following we restrict our attention to (symmetric) initial data on a neighborhood of $[-e^{-t_0}, e^{-t_0}]$ and consider the evolution of that data on its domain of dependence.

A solution $S(t, z)$ with initial data sufficiently close (in, e.g., a $\mathcal{C}^{k,\alpha}$ norm) to an explicit spike transition $\mathcal{T}_{\mathsf{Hi}}$ will remain close to that solution for some time interval; temporarily we may thus speak of an *approximate spike transition*. The solution $S(t, z)$ is approximated by $\mathcal{T}_{\mathsf{Hi}}$ at least up to a point when the two solutions reach a neighborhood of the Kasner circle $\mathrm{K}^{\bigcirc}$. While $\mathcal{T}_{\mathsf{Hi}}$ continues to converge to a fixed point on $\mathrm{K}^{\bigcirc}$, the solution $S(t, z)$ will, in general, stray off course—it ceases to be an approximate spike transition. The initially small deviation of $S(t, z)$ from $\mathcal{T}_{\mathsf{Hi}}$ amplifies (in the sense of increasing relative errors) and leads to different behavior in the variable $R_3$. In contrast to $\mathcal{T}_{\mathsf{Hi}}$, this variable is triggered at $\mathrm{K}^{\bigcirc}$ and $S(t, z)$ undergoes an approximate $\mathcal{T}_{R_3}$ frame transition. This behavior can be understood, qualitatively and quantitatively, by considering a linearization of the equations at $\mathrm{K}^{\bigcirc}$, but since such an analysis goes beyond the scope of the present paper it will be pursued elsewhere. For the present purposes we restrict ourselves to referring to the strong numerical evidence we have obtained for the described behavior: The numerics suggest that the solution $S(t, z)$ shadows an OT spike chain

$$\mathcal{T}_{\mathsf{Hi}} \to \mathcal{T}_{R_3} \to \cdots \to \mathcal{T}_{\mathsf{Hi}} \to \mathcal{T}_{R_3} \to \begin{cases} \mathcal{T}_{\mathsf{Hi}} \\ - \\ \mathcal{S}_{\mathsf{Lo}} \\ \mathrm{Bill} \end{cases}, \quad (46)$$

and thus $S(t, z)$ is an *approximate OT spike chain*. Furthermore, the numerical evidence shows that an approximate OT spike chain $\mathcal{S}$ shadows an exact OT spike chain with an increasing degree of accuracy; in particular, the asymptotic limit of $S(t, z)$ is a small perturbation of the limit of the OT spike chain itself.

For an approximate spike transition we *define* its (inverse) spike width $c_z$ through (42), i.e.,

$$c_z = \frac{1 + 2\tilde{p}_1|_{z=0}}{24\tilde{p}_1|_{z=0}} (\check{u}_- + f(\check{u}_-)\tilde{p}_1|_{z=0})^{-\check{u}_-/w}$$
$$\times (-\check{u}_+ - f(\check{u}_+)\tilde{p}_1|_{z=0})^{\check{u}_+/w} \partial_z N_1|_{z=0}, \quad (47)$$

where we recall that $\tilde{p}_1 = \frac{1}{3}(1 + \Sigma_1)$. The inverse width $c_z$ of an approximate spike transition will in general not be a constant exactly, but depend on when (47) is evaluated.

However, for an approximate spike transition, $c_z$ will be approximately constant, at least up to the point where the deviation from $\mathcal{T}_{\mathsf{Hi}}$ becomes too large. Note that definition (47) is not unique in the sense that it can be replaced by similar definitions involving, e.g., $N_{12}$ and $\tilde{p}_2$ instead of $N_1$ and $\tilde{p}_1$. Evidently, for exact spike transitions this does not cause any difference, while for approximate spike transitions the resulting value will indeed differ from (47) in general. However, the slight ambiguities quickly converge to zero when the approximate spike transitions are approximated by the exact transitions with an increasing degree of accuracy.

Considering an approximate OT spike chain $S(t, z)$ a natural question to ask concerns the behavior of the evolution of the spike width. Suppose that $S(t, z)$ is approximated for some time interval by an exact spike transition $\mathcal{T}_{\mathsf{Hi}}$ with parameter $\check{u}_0$, inverse width $c_0$, and time offset $-t_0$, i.e., by (29) with the replacements $z \mapsto c_0 z$ and $t \mapsto t - t_0$. In a (much) later time interval, the solution $S(t, z)$ is then approximated by the subsequent $\mathcal{T}_{\mathsf{Hi}}$ of the chain; we have $\check{u}_1 = \check{u}_0 - 2$, inverse coordinate width $c_1$, and time offset $t_1$ (where $t_1 \gg t_0$). In Appendix E we show that

$$c_1 = e^{t_1 - t_0} c_0 = e^{\Delta t} c_0. \quad (48)$$

The time $\Delta t$ between two subsequent (approximate) spike transitions is dominated by the time the solution spends in the neighborhood of $\mathrm{K}^{\bigcirc}$. The closer the solution $S(t, z)$ is to an exact OT spike chain, the greater $\Delta t$ will be. As a consequence the coordinate width of the spike decreases rapidly toward the singularity, since the inverse width increases rapidly.

## V. CONCATENATION IN THE GENERAL $G_2$ CASE

In contrast to the OT case, the Hubble-normalized frame variable $R_1$ does not vanish identically for the general $G_2$ models. As a consequence, sector (312), which is stable for the OT models, see Fig. 7(a), possesses an unstable manifold which is associated with the variable $R_1$, see Fig. 10. The same is true for the part of sector (132) with $0 < \check{u} < 1/2$, which is stable for the spike surface



(a) Triggers for BKL chains
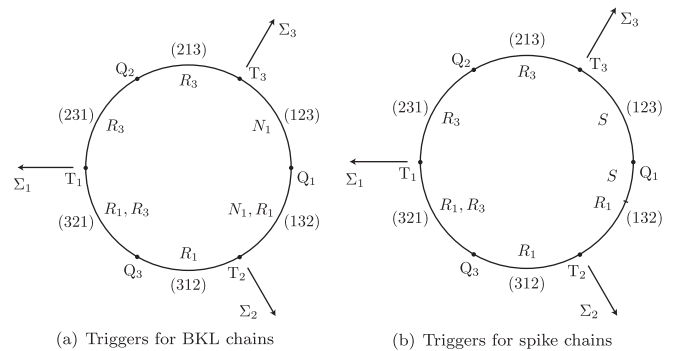
(b) Triggers for spike chains

FIG. 10. Triggers for general $G_2$ models. Figures (a) and (b) generalize Figs. 7(a) and 9, respectively.

trajectories in the OT context, see Fig. 9, but unstable through $\mathcal{T}_{R_1}$ frame transitions for general $G_2$ models; see Fig. 10(a). Intuitively it follows that the instability of the entire Kasner circle (except for, possibly, the Taub points) prevents convergence of (generic) solutions to generalized Kasner solutions and leads to *oscillatory singularities*. In this section we present analytical and numerical evidence that corroborate this conjecture.

### A. BKL concatenation and BKL chains

Concatenation of frame transitions $\mathcal{T}_{R_1}$, $\mathcal{T}_{R_3}$, and curvature transitions $\mathcal{T}_{N_1}$ yields heteroclinic chains, which we refer to as a *BKL chains*; see Fig. 11. As opposed to OT chains, BKL chains are *infinite* in general.

Note that in the present case a BKL chain is not uniquely determined by an (initial) fixed point on $\mathrm{K}^{\bigcirc}$. This is because there are two sectors with two triggers (i.e., unstable modes) instead of one; see Fig. 10. In sector (132) it is possible to continue the chain with a $\mathcal{T}_{N_1}$ curvature transition or a $\mathcal{T}_{R_1}$ frame transition; in sector (321) it is possible to continue with a $\mathcal{T}_{R_1}$ or a $\mathcal{T}_{R_3}$ frame transition, but after two or three transitions different paths rejoin again; see Fig. 11. We will discuss the scenario of two triggers at a fixed point further below, but before doing so it is of interest to compare the situation with the mixmaster case associated with Bianchi types VIII and IX. Recall that the symmetry adapted frames of types VIII and IX are not of the Iwasawa type; instead it is strongly preferable to use a symmetry group compatible Fermi propagated orthonormal frame, which yields three types of curvature transitions associated with the three spatial directions, while frame transitions are absent. Thus, in contrast with
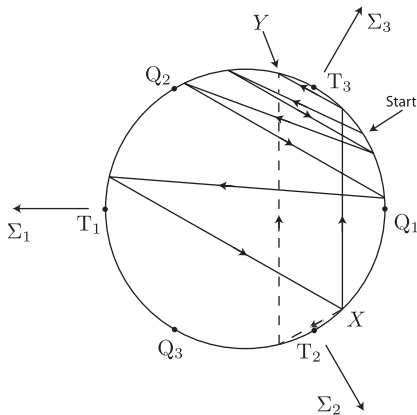


FIG. 11. A BKL chain is an (in general) infinite heteroclinic chain consisting of $\mathcal{T}_{N_1}$, $\mathcal{T}_{R_1}$ and $\mathcal{T}_{R_3}$ curvature and frame transitions. The paths are not unique; e.g., at the point $X$ two continuations are possible, a frame transition $\mathcal{T}_{R_1}$ or a curvature transition $\mathcal{T}_{N_1}$ (dashed line). However, the different paths rejoin at the point $Y$ after an additional curvature-frame transition. At the point $Y$ the chain continues with a (not shown) $\mathcal{T}_{R_3}$ transition.

the present case, the associated BKL chains do not exhibit the ambiguities of Fig. 11; see, e.g., Ref. [44] for details.

In analogy with the role of OT BKL chains in the OT context, the relevance of BKL chains in the present context is twofold. On the one hand, the role of BKL chains for spatial homogeneous models is immediate: Since the symmetry-adapted frames of general Bianchi type $\mathrm{VI}_{-1/9}$ models are Iwasawa frames, these models are of the form (1) where the metric is manifestly spatially homogeneous; see Ref. [51]. The asymptotic evolution toward the initial singularity of general type $\mathrm{VI}_{-1/9}$ models is expected to be represented by[7] BKL chains which lead to infinite oscillations between different Kasner states; the singularity can therefore be referred to as being *oscillatory*. On the other hand, there exists heuristic evidence [51] and numerical support [53,55] that the asymptotic evolution towards a generic spacelike singularity along a generic (open) set of time lines of a general inhomogeneous vacuum (or "vacuum dominated") solution of the Einstein equations (with $|N_1 R_1 R_3| > 0$) is represented by BKL chains as well. (For the perfect fluid case and "vacuum dominance" we refer to Ref. [68] and references therein.)

Asymptotic shadowing necessarily brings solutions (e.g., type $\mathrm{VI}_{-1/9}$ solutions or single time lines of inhomogeneous solutions) to a neighborhood of a Kasner point where two variables are triggered (i.e., grow exponentially). Consider, e.g., the case of a trajectory following a $\mathcal{T}_{R_3}$ transition to a fixed point $X$ on sector (132) of $\mathrm{K}^{\bigcirc}$, where $N_1$ and $R_1$ are triggers, see Figs. 10 and 11. If $|N_1| \ll |R_1|$ ($\ll 1$) when the trajectory enters a neighborhood of the fixed point $X$, $R_1$ will be triggered and a $\mathcal{T}_{R_1}$ will follow; if $|R_1| \ll |N_1|$, $N_1$ will be triggered and a $\mathcal{T}_{N_1}$ will follow. Clearly, it is possible to prescribe initial data such that both $R_1$ and $N_1$ grow to macroscopic size, which means that a so-called multiple transition (here, a mixed curvature-frame transition) follows. Generic BKL chains enter a neighborhood of the fixed point $X$ infinitely many times, and generic solution trajectories are thus expected to do likewise. However, the analysis of Ref. [51] suggests that the multiple transition scenario does not occur generically in a statistical sense; in the asymptotic limit, trajectories usually follow single transitions (and thus BKL chains), a result that is consistent with the billiard picture of Damour *et al.* [52]. The question of which of the two possible transitions, $\mathcal{T}_{R_1}$ or $\mathcal{T}_{N_1}$, is followed more frequently, is delicate. Linearization of the system at $X$ yields the eigenvalues associated with the variables $R_1$ and $N_1$. If the eigenvalue associated with, say, $R_1$ is

---

[7]The exact meaning of "being represented by" is a delicate point. Clearly, the evolution of initial data close to a Kasner point is approximately described, at least for a finite time, by a finite piece of a BKL chain ("finite shadowing"). However, the study of mixmaster dynamics [45–48] suggests the possibility that a generic solution asymptotically follows its BKL chain forever.

considerably larger than the other, triggering a $\mathcal{T}_{R_1}$ transition seems more likely than a $\mathcal{T}_{N_1}$ transition. It is possible, however, that $R_1$ is almost always sufficiently small against $N_1$ when the trajectory comes close to $X$, which would make $\mathcal{T}_{N_1}$ transitions more frequent than expected. In any case, the fact that different paths rejoin, makes the ambiguity in paths a transient problem.

### B. Spike concatenation in the general $G_2$ models

While the oscillatory asymptotic dynamics of generic time lines is represented by BKL chains, the evolution of spike time lines, and their neighbors, bears no relation to spatially homogeneous dynamics; the BKL picture breaks down. This is because $N_1$ is zero at the spike surface which results in a loss of the trigger $N_1$ in sectors (123) and (132); in other words, $\mathcal{T}_{N_1}$ curvature transitions cannot take place. However, from Fig. 10(a) we see that the general $G_2$ case has at least one trigger at each sector of $K^\circ$ (which is due to the existence of a nonzero $R_1$), where spatial gradients take the role as triggers in sector (123) and part of sector (132). We will argue that this "instability" of the Kasner circle results in oscillatory dynamics which is represented by infinite spike chains.

As in the case of OT spike chains, see Sec. IV C, high velocity spike transitions $\mathcal{T}_{Hi}$ and single $\mathcal{T}_{R_1}$ and $\mathcal{T}_{R_3}$ frame transitions can be concatenated straightforwardly since the entire family of curves representing a $\mathcal{T}_{Hi}$ converges to a point on $K^\circ$ as $t \to -\infty$ and to another point on $K^\circ$ as $t \to \infty$. However, the situation for low velocity spike solutions $\mathcal{S}_{Lo}$ is different, because the limit on $K^\circ$ of the trajectory of the spike surface $z = 0$ differs from the (common) limit of the $z \neq 0$ time lines; see Figs. 4(d) and 5. It is obvious that low velocity spike solutions $\mathcal{S}_{Lo}$ do not immediately fit into the network of transitions, and neither does the Bill spiky feature discussed in Sec. III E for similar reasons.

However, we will see that low velocity spike solutions naturally *combine* with a frame rotation in $R_1$ and part of a high velocity transition to form a *joint low or high velocity spike transition* which we denote by $\mathcal{T}_{Jo}$ (a similar comment also holds for the Bill spiky feature due to that it can be described as the second half of a $\mathcal{S}_{Lo}$ spike solution; because of the close relationship between $\mathcal{S}_{Lo}$ solutions and Bill spiky features we will for brevity here focus on $\mathcal{T}_{Jo}$). The spike transitions $\mathcal{T}_{Jo}$ are characterized by the same fundamental property as $\mathcal{T}_{Hi}$ transitions that the entire family of curves representing a $\mathcal{T}_{Jo}$ transition emerges from one point and ends at another point on $K^\circ$, and it is for this reason $\mathcal{T}_{Jo}$ and not $\mathcal{S}_{Lo}$ is the natural concatenation building block. There is thus a stark contrast between the OT case and the general $G_2$ case. In the OT case a $\mathcal{S}_{Lo}$ solution and perturbations thereof develop permanent spatial structures since the time lines of the spike surface and the nonspike time lines converge to two different Kasner points, see Figs. 4(d) and 5; in the

general $G_2$ case these spatial structures form *and unform* and hence $\mathcal{S}_{Lo}$ *is merely the first part of the transition* $\mathcal{T}_{Jo}$: The time lines rejoin eventually. In general, spikes are transient recurring features. Furthermore, we will see that the initial Kasner point and the final Kasner point of a joint low or high velocity spike transition $\mathcal{T}_{Jo}$ are related by the spike map (35′), which thus characterizes *both* $\mathcal{T}_{Hi}$ and $\mathcal{T}_{Jo}$ transitions, a property, as we will argue, that is not coincidental.

In order to unveil the structures leading to joint low or high velocity spike transitions $\mathcal{T}_{Jo}$ we use information about *timing*. First, consider Fig. 4(d) and compare the trajectory of the spike surface $z = 0$ with the trajectories associated with $z \neq 0$ of a neighborhood $U_0$ of $z = 0$ of $\mathcal{S}_{Lo}$. The (dashed) lines of constant time show that the respective final Kasner points, $A_0$ and $A_1$, are approached "simultaneously" (which is in contrast to the approach to the initial Kasner state); specifically, let $X(t, z)$ denote the family of curves representing the $\mathcal{S}_{Lo}$ transition; then $|X(t, 0) - A_0|$ and $|X(t, 1) - A_1|$ are of the same order as $t \to \infty$. Furthermore, for $t \gg 1$, the set $\{X(t, z) | z \in U_0\}$ is approximated by the straight line $S_A$ connecting the two Kasner points $A_0$ and $A_1$, which corresponds to the $\mathcal{T}_{N_1}$ transition that originates from $A_0$; see Fig. 5.

Second, consider Figs. 4(a) or 4(b); let $Y(t, z)$ denote the family of curves representing the $\mathcal{T}_{Hi}$ transition. The convergence as $t \to -\infty$ to the initial Kasner point $B_0$ is nonuniform; the (dashed) lines of constant time show that for $t \ll -1$, the set $\{Y(t, z) | z \in \mathbb{R}\}$ is approximated by the straight line $S_B$ representing the $\mathcal{T}_{N_1}$ transition connecting the initial Kasner point $B_0$ with the Kasner point $B_1$.

In the general $G_2$ case the variable $R_1$ does not vanish identically. Consider initial data generated by a small perturbation of $\mathcal{S}_{Lo}$ initial data such that $|R_1| \neq 0$ is sufficiently small. (In accordance with the considerations of Sec. IV C we assume symmetric initial data sets; in particular, $R_1$ is an even function of $z$.) The associated solution $S(t, z)$ shadows the $\mathcal{S}_{Lo}$ transition closely; hence, for a large $t_A$, $\{S(t_A, z) | z\} \approx S_A$. However, $S(t, z)$ cannot converge to the Kasner circle since $R_1$ increases in a neighborhood of $S_A$, cf. Fig. 10. Eventually, despite the initial smallness of $R_1$, the solution $S(t, z)$ will be transported away from $S_A$ by a "frame transition."

A trajectory $\{S(t, \bar{z}) | t\}$ with sufficiently large $|\bar{z}|$ (i.e., sufficiently far from the spike surface) is approximated by a BKL chain: While $S(t, \bar{z})$ approaches the Kasner point $A_1$, $R_1$ grows steadily and a $\mathcal{T}_{R_1}$ frame transition follows, i.e., $S(t, \bar{z}) \approx \mathcal{T}_{R_1}$ for some time interval, which brings $S(t, \bar{z})$ into the vicinity of the Kasner point $B_1$, where $R_1$ decreases rapidly; from there a $\mathcal{T}_{R_3}$ frame transition ensues taking $S(t, \bar{z})$ to the Kasner point $C_0$ where the trigger $N_1$ induces a $\mathcal{T}_{N_1}$ curvature transition that eventually takes $S(t, \bar{z})$ to a Kasner point $C_1$. For the trajectory $\{S(t, 0)|, t\}$ representing the spike surface, the scenario is straightforward as well:
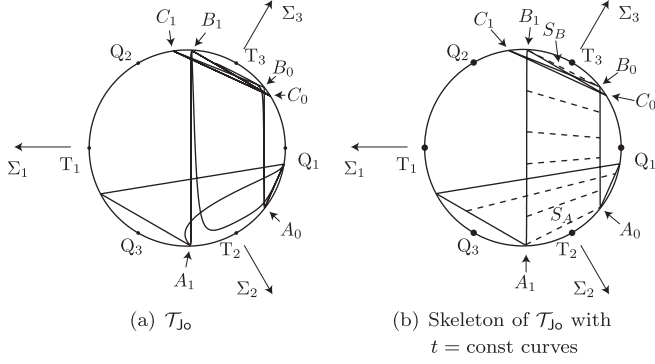
(a) $\mathcal{T}_{\mathsf{Jo}}$

(b) Skeleton of $\mathcal{T}_{\mathsf{Jo}}$ with $t = \text{const}$ curves

FIG. 12. A joint low or high velocity spike transition $\mathcal{T}_{\mathsf{Jo}}$ consists of a low velocity spike solution $\mathcal{S}_{\mathsf{Lo}}$ followed by a family of $\mathcal{T}_{R_1}$ frame transitions and the "second part" of a high velocity spike transition $\mathcal{T}_{\mathsf{Hi}}$. In (a) we depict the numerical evolution of four time lines associated with different values of $z$ from $z = 0$ (spike surface trajectory) to $|z| \gg 1$ (BKL chain). Subfigure (b) shows the curves of constant time (dashed lines) for a $\mathcal{T}_{\mathsf{Jo}}$, which correspond to segments of the straight lines representing $\mathcal{T}_{N_1}$ transitions.

$S(t, 0)$ approaches the Kasner point $A_0$ while $R_1$ grows steadily; a $\mathcal{T}_{R_1}$ frame transition follows, which brings $S(t, 0)$ into the vicinity of the Kasner point $B_0$ (where $R_1$ decreases rapidly); a spike surface trajectory $\mathcal{T}_S$ follows and the solution approaches the Kasner point $C_1$; in particular we observe that $S(t, 0)$ *rejoins* $S(t, \tilde{z})$ at $C_1$; we refer to Fig. 12. The described scenario is supported by heuristic arguments invoking Fig. 10(a) and the symmetry of the initial data set, and by numerical simulations, exemplified in Figs. 12(a) and 12(b).

Numerical experiments provide further information: For $t > t_A$, the solution $S(t, z)$ is transported from $S_A$ to $S_B$, i.e., there is $t_B > t_A$ such that $\{S(t_B, z)|z\} \approx S_B$; see Figs. 12(a) and 12(b). Note that $R_1$ is decreasing rapidly as the solution approaches $S_B$. The transition from $S_A$ to $S_B$ occurs in a special manner: Curves of constant time, i.e., $\{S(t, z)|z\}$, $t_A < t < t_B$, see the dashed lines of Fig. 12(b), are straight lines corresponding to segments of the paths of $\mathcal{T}_{N_1}$ curvature transitions. The frame transition that maps $S(t_A, z)$ to $S(t_B, z)$ is therefore the (nonlinear) superposition of two motions: The motion represented by the "ladder" of constant time slices of Fig. 12(b) and the motion of spatial points along $t = \text{const}$ lines. For $t$ close to $t_A$, (32a′) yields

$$\tilde{p}_1 = \frac{-\check{u}_A(1 - k_A^2 e^{4\check{u}_A(t-t_A)} z^2)}{f(\check{u}_A) + f(-\check{u}_A)k_A^2 e^{4\check{u}_A(t-t_A)} z^2}, \tag{49a}$$

where $k_A$ is a constant and $\check{u}_A$ is associated with the Kasner point $A_0$; (49a) describes the motion of spatial points $z$ along $S_A$ for $t$ close to $t_A$. [Note the intimate connection of (49a) with a Bill spiky feature; see Sec. III E]. For $t$ close to $t_B$, on the other hand, we have

$$\tilde{p}_1 = \frac{-\check{u}_B(1 - k_B^2 e^{4\check{u}_B(t-t_B)} z^2)}{f(\check{u}_B) + f(-\check{u}_B)k_B^2 e^{4\check{u}_B(t-t_B)} z^2}$$

$$= \frac{-\check{u}_A(1 - k_B^2 e^{4\check{u}_B(t-t_B)} z^2)}{f(\check{u}_A) + f(-\check{u}_A)k_B^2 e^{4\check{u}_B(t-t_B)} z^2}, \tag{49b}$$

where $k_B$ is another constant and $\check{u}_B$ is associated with $B_0$, i.e., $\check{u}_B = \check{u}_A^{-1}$ (because $\check{u}_B$ arises from $\check{u}_A$ through a $\mathcal{T}_{R_1}$ transition). Equation (49b) describes the motion of spatial points along $S_B$ when $t$ is close to $t_B$. Interpolation between the two motions (49a) and (49b) (qualitatively) leads to the trajectories observed numerically, an example being the curve connecting $A_0$ with $B_1$ in Fig. 12(a). The remaining (and crucial) question concerns the evolution for $t > t_B$. The numerical simulations show that the solution $S(t, z)$ continues as an approximate high velocity transition $\mathcal{T}_{\mathsf{Hi}}$ for $t > t_B$ (while $R_1$ continues to decrease). In particular, we find that the entire family of trajectories $S(t, z)$ rejoins at the final point $C_1$ of the $\mathcal{T}_{\mathsf{Hi}}$ transition.

Figures 12(a) and 12(b) summarize the considerations and give depictions of a joint low or high velocity spike transition $\mathcal{T}_{\mathsf{Jo}}$. We reemphasize the property that the $t = \text{const}$ curves are straight lines that coincide with the paths of $\mathcal{T}_{N_1}$ curvature transitions. This 'timing' property shows that the spiky structure that forms under an (approximate) $\mathcal{S}_{\mathsf{Lo}}$ is transported by a $R_1$ frame rotation to the spiky structure appearing in (the middle of) an (approximate) $\mathcal{T}_{\mathsf{Hi}}$ and eventually unforms according to the $\mathcal{T}_{\mathsf{Hi}}$ evolution.

A joint low or high velocity spike transition $\mathcal{T}_{\mathsf{Jo}}$ induces a map between the initial and the final Kasner state of the transition,

$$\mathcal{T}_{\mathsf{Jo}}: \check{u}_- \overset{\mathcal{S}_{\mathsf{Lo}}}{\mapsto} \begin{Bmatrix} 1 - \check{u}_- \\ \check{u}_- - 1 \end{Bmatrix} \overset{\mathcal{T}_{R_1}}{\mapsto} \begin{Bmatrix} \frac{1}{1-\check{u}_-} & \overset{\mathcal{T}_{\mathsf{Hi}}}{\mapsto} \\ \frac{1}{\check{u}_- - 1} & \overset{\mathcal{T}_{R_3}}{\mapsto} \frac{\check{u}_-}{1-\check{u}_-} \overset{\mathcal{T}_{N_1}}{\mapsto} \end{Bmatrix}$$

$$\mapsto -\frac{\check{u}_-}{1 - \check{u}_-}, \tag{50a}$$

which, in terms of the standard Kasner parameter coincides with the spike map (35′) of $\mathcal{T}_{\mathsf{Hi}}$ transitions. The connection between $\mathcal{T}_{\mathsf{Hi}}$ and $\mathcal{T}_{\mathsf{Jo}}$ transitions is even stronger: Consider Fig. 14. On the one hand, the Kasner point $O$ in sector (132) with $1/2 < \check{u} < 1$ is the initial point of a joint low or high velocity spike transition $\mathcal{T}_{\mathsf{Jo}}$; on the other hand, there is a $\mathcal{T}_{R_1}$ frame transition emerging from $O$, which can be continued with a high velocity transition and another $\mathcal{T}_{R_1}$ frame transition; the finite chain $\mathcal{T}_{R_1}$-$\mathcal{T}_{\mathsf{Hi}}$-$\mathcal{T}_{R_1}$ yields

$$\check{u}_- \overset{\mathcal{T}_{R_1}}{\mapsto} \frac{1}{\check{u}_-} \overset{\mathcal{T}_{\mathsf{Hi}}}{\mapsto} -\frac{1 - \check{u}_-}{\check{u}_-} \overset{\mathcal{T}_{R_1}}{\mapsto} -\frac{\check{u}_-}{1 - \check{u}_-} = \check{u}_+, \tag{50b}$$

hence the final state of the chain $\mathcal{T}_{R_1}$-$\mathcal{T}_{\mathsf{Hi}}$-$\mathcal{T}_{R_1}$ coincides with the final state of the joint low or high velocity spike transition $\mathcal{T}_{\mathsf{Jo}}$. This corroborates that $\mathcal{T}_{\mathsf{Jo}}$ and $\mathcal{T}_{\mathsf{Hi}}$ are

(a) Spike chain with two $\mathcal{T}_{\mathsf{Hi}}$ transitions

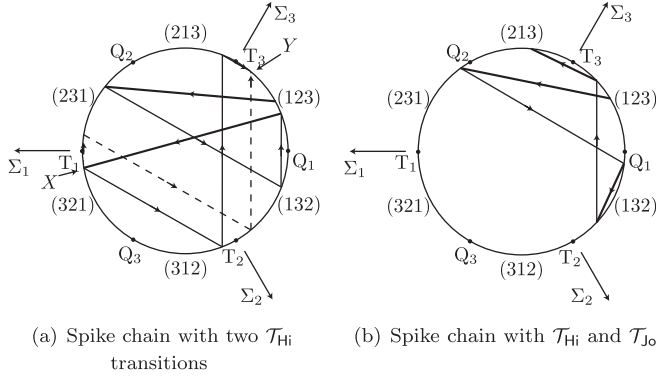(b) Spike chain with $\mathcal{T}_{\mathsf{Hi}}$ and $\mathcal{T}_{\mathsf{Jo}}$

FIG. 13. Examples of (parts of) spike chains. In (a) the continuous lines represent the spike time line ($z = 0$ trajectory) of $\mathcal{T}_{\mathsf{Hi}}$-$\mathcal{T}_{R_3}$-$\mathcal{T}_{R_1}$-$\mathcal{T}_{\mathsf{Hi}}$-$\mathcal{T}_{R_3}$-$\mathcal{T}_{R_1}$-$\mathcal{T}_{R_3}$; the dashed lines are $\mathcal{T}_{R_1}$-$\mathcal{T}_{R_3}$-$\mathcal{T}_{R_1}$. In (b) we have $\mathcal{T}_{\mathsf{Hi}}$-$\mathcal{T}_{R_3}$-$\mathcal{T}_{\mathsf{Jo}}$ (where $\mathcal{T}_{\mathsf{Jo}}$ consists of three pieces: $\mathcal{S}_{\mathsf{Lo}}$-$\mathcal{T}_{R_1}$-$\mathcal{T}_{\mathsf{Hi}}$).

structures that are on an equal footing (through additional $R_1$ frame rotations).

A spike chain is an in general infinite concatenation of spike transitions and frame transitions; the "chain links" are high velocity spike transitions $\mathcal{T}_{\mathsf{Hi}}$ and joint low or high velocity spike transitions $\mathcal{T}_{\mathsf{Jo}}$ and $\mathcal{T}_{R_1}$ and $\mathcal{T}_{R_3}$ frame transitions.[8] Examples of (short parts of) spike chains are given in Fig. 13. The role of spike chains for the dynamics of (generic) $G_2$ models is suggested by numerical experiments: Asymptotically, solutions $S(t, z)$ are *approximate spike chains*, i.e., solutions shadow spike chains (with an increasing degree of accuracy). The role of spike chains for generic $G_2$ models is thus exactly analogous to the role of BKL chains for spatially homogeneous models.

These considerations strongly suggest that the permanent asymptotic spike features ("permanent spikes") of OT models such as the $T^3$ Gowdy models, which have been emphasized in the literature, are *irrelevant* for general $G_2$ models and generic singularities: The permanent features of OT models are "mutilated" halves of transient, and recurring, spike transitions in the generic context, and thus quite misleading. Spatial structures form and unform recurrently; however, during these oscillations, the spike widths shrink to zero size, thus leading to quite different nonuniform features than in the OT case. Oscillations are oscillations between Kasner states; the asymptotic dynamics of a spike time line is represented by the spike trajectory ($z = 0$) of a spike chain; the asymptotic dynamics of a generic spatial point is represented by a BKL chain (which corresponds to the trajectory on the 'boundary' $|z| = \infty$ of a spike chain).

---

[8]As discussed in Sec. III E, a Bill spiky feature can be regarded as the second half of a $\mathcal{S}_{\mathsf{Lo}}$ solution. As a consequence a Bill spiky feature in the general case can be viewed as part of a $\mathcal{T}_{\mathsf{Jo}}$ transition that begins approximately at $S_A$ with $A_0$ as common initial Kasner point and $C_1$ as common final Kasner point.
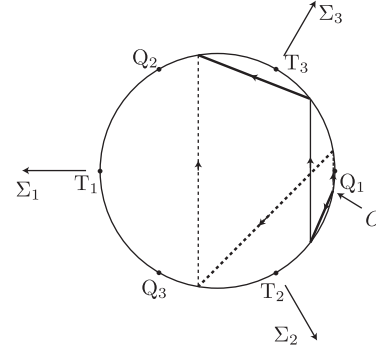


FIG. 14. A Kasner point $O$ in sector (132) with $1/2 < \check{u} < 1$ is the initial point of a joint low or high velocity spike transition $\mathcal{T}_{\mathsf{Jo}}$ (where the continuous line represents the time line of the spike surface); however, there is also a $\mathcal{T}_{R_1}$ frame transition emerging from $O$, which can be continued with a $\mathcal{T}_{N_1}$ curvature transition and another $\mathcal{T}_{R_1}$ frame transition. The two trajectories meet at the same final Kasner point.

We conclude with two remarks. First, consider Fig. 14 and recall that the final state of a low or high velocity spike transition $\mathcal{T}_{\mathsf{Jo}}$ and the chain $\mathcal{T}_{R_1}$-$\mathcal{T}_{\mathsf{Hi}}$-$\mathcal{T}_{R_1}$ coincide. It is highly plausible that "mixed" (or "double") transitions exist, in close analogy with, e.g., double frame transitions (involving $R_1$ and $R_3$ at the same time) and mixed curvature-frame transitions (involving $N_1$ and frame variables at the same time); see Ref. [51]. This further stresses the close relationship between $\mathcal{T}_{\mathsf{Jo}}$ and $\mathcal{T}_{\mathsf{Hi}}$ and identifies $\mathcal{T}_{\mathsf{Jo}}$ and $\mathcal{T}_{R_1}$-$\mathcal{T}_{\mathsf{Hi}}$-$\mathcal{T}_{R_1}$ as the limiting cases (boundary) of an entire family of transitions. However, by analogy with the case of double frame and mixed curvature-frame transitions we expect that, asymptotically and generically, merely the single spike transitions, $\mathcal{T}_{\mathsf{Jo}}$ and $\mathcal{T}_{\mathsf{Hi}}$, will occur in a spike chain. Second, we note that in the spatially homogeneous Bianchi types $VI_{-1/9}$, VIII, and IX, solutions cannot converge to Kasner states (other than the Taub points—in the LRS case); all solutions are oscillatory. We expect (almost) the same to be true in the general $G_2$ case: While in the OT case, solutions converge to generalized Kasner states, we expect that (almost) all solutions are oscillatory in the general $G_2$ case.

## VI. CONCLUDING REMARKS

In this paper we have discussed the asymptotic dynamics of $G_2$ models toward a singularity. We have given heuristic arguments and strong numerical evidence showing that the well-known permanent spatial structures (spikes) arising in special models such as the $T^3$ Gowdy models are absent in general $G_2$ models: General $G_2$ models possess oscillatory singularities, which are characterized by BKL oscillations *and* the recurring formation and unformation of spiky features whose width rapidly shrinks towards the singularity; the asymptotic dynamics is represented by infinite BKL and spike chains and is thus associated with two types of sequences of Kasner epochs.

The world line of the spike surface is characterized by an oscillation between Kasner epochs induced by the map that in terms of the gauge-invariant Kasner parameter $u$ is given by

$$u \rightarrow \begin{cases} u - 2 & u \in [3, \infty) \\ (u - 2)^{-1} & u \in [2, 3] \\ ((u - 1)^{-1} - 1)^{-1} & u \in [3/2, 2] \\ (u - 1)^{-1} - 1 & u \in [1, 3/2], \end{cases} \quad (51)$$

which is in contrast to the usual Kasner map

$$u \rightarrow \begin{cases} u - 1 & u \in [2, \infty) \\ (u - 1)^{-1} & u \in [1, 2]. \end{cases} \quad (52)$$

In a subsequent paper [71], we will we analyze statistical properties of the Kasner oscillations of spike world lines by investigating the map (51) in detail.

Although we expect that nonlocal (i.e., non-BKL) dynamics will be asymptotically confined to spike surfaces, which is due to the rapidly shrinking spike widths, and that these spike surfaces constitute a set of measure zero of all spatial points, an understanding of recurring spikes is still crucial for our understanding of generic spacelike singularities:

(i) The key solutions that describe BKL and non-BKL behavior are intimately related with each other through solution generating algorithms, which create a hierarchical order for these solutions; this strongly hints at the existence of hidden symmetries, which are thus a common theme in our quest to understand generic spacelike singularities.[9] The case for hidden symmetries is further strengthened by the observation that the 'spatial boundary' (i.e., $|z| \to \infty$) of the spike chains are the BKL chains. Since the spike surface trajectories (non-BKL dynamics) meet the trajectories of the other spatial points (BKL dynamics) periodically, there is a close relation between the map (51) and the Kasner map (52). Accordingly, the BKL scenario seems to be part of a greater picture which is needed for a complete understanding of generic singularities.

_____

[9]The solution generating techniques used to obtain the spike solutions in a hierarchical manner involve the OT line element in an Iwasawa frame, i.e., (45), and in the area time gauge. The solutions are obtained by alternately applying the so-called Gowdy-to-Ernst (GE) transformation and a certain frame rotation (FR) which is obtained by a rotation of the symmetry coordinates $x$ and $y$ by $-\pi/2$. Starting with the Kasner solution in diagonal form and performing a GE transformation yields the Kasner solution in nontrivial OT form; a FR yields the frame rotated Kasner solution associated with $\mathcal{T}_{R_3}$; subsequent application of a GE transformation gives the Bianchi type II vacuum solution in a Fermi frame; applying the FR again yields a "spikily rotating" Bianchi type II vacuum solution, known as a false spike solution; acting on this with the GE transformation results in the explicit spike solution; for details, see Ref. [56].

(ii) Proofs about generic spacelike singularities *must* take into account recurring spikes, since estimates (e.g., of spatial derivatives) are heavily affected.

(iii) Spikes are associated with the zeros of certain functions (e.g., the variable $N_1$). Special initial data (like the symmetric data considered in this paper) can fix the location of a spike; however, in general, spikes need not be present initially but will form when a function goes through zero and move in accordance with the evolution of the functions and its zero(s). Unfortunately, this does not answer the question of what the *physical* reasons for spike *formation* are. Our lack of knowledge and intuition for spike formation prevents us from even an educated guess about how many spikes form generically. At the moment we cannot exclude that a dense set of spikes can form toward generic spacelike singularities. BKL asymptotic dynamics would still be generic, but the BKL scenario would certainly obtain an unexpectedly significant non-BKL counterpart.

Let us turn to numerical issues. At present, numerical accuracy regarding the simulation of spikes can be categorized into three levels:

(i) At the crudest level of numerical accuracy there are not enough grid points to simulate spikes correctly; moreover, spikes are artificially produced and annihilated.

(ii) At the intermediate level of numerical accuracy there are enough grid points to accurately describe one spike transition correctly, but numerical convergence is not achieved for simulations that are supposed to follow a concatenation of spike transitions. The first indication of nonconvergence is the difference in the timing of transitions. The intermediate level yields quantitatively correct results for simulations of one spike transition, and qualitatively correct results for simulations of short parts of spike chains.

(iii) Finally, at the highest level of numerical accuracy there are enough grid points to obtain numerical convergence for longer simulations that cover parts of spike chains. But even these simulations are currently limited to two or three spike transitions. We are confident that improvement can come from the insights gained in this paper.

With the benefit of hindsight we are in a position to reproduce and assess what was actually achieved in the numerical simulations of different papers. Early numerical work on spiky features has to be considered as having crude numerical accuracy, thus belonging to the first category, but it nevertheless managed to tie spiky features to analytic conditions in special models such as the $T^3$ Gowdy models, as exemplified in Ref. [27]. Hern [33] and Berger *et al.* (see Ref. [10] and references therein) also studied general $G_2$ models with $T^3$ topology numerically, but again, even though Hern used mesh refinement, numerical

accuracy was not sufficient to resolve several spike transitions correctly. (Hern also simulated spikes in models with a single spacelike Killing vector [33], which is an even harder numerical problem.) It was not until 2003 that the first qualitatively correct spike simulation was done by Garfinkle and Weaver [38] in the case of $T^3$ Gowdy models, described by means of $P_{,\tau}$ and the speed $v$ [see Appendix D and Fig. 8 for a description in terms of projections on $(\Sigma_1, \Sigma_2, \Sigma_3)$ space]. The first qualitatively correct spike simulation in the general $G_2$ case was first done in 2005 by Andersson *et al.* [53]. This qualitative picture was confirmed quantitatively and linked to Lim's explicit solutions [56] in 2009 by Lim *et al.* [57]. The key idea to simulate several spike transitions accurately was to use the explicit spike solutions to design a grid that zoomed in on a single recurring spike. Despite this, only a few high (but no low) velocity spike transitions were followed.

The work [57] makes it clear what a formidable numerical challenge recurring spikes pose. It is important to note that all quantitatively correct spike simulations so far involve recurring spikes that are forced by special initial conditions to be fixed in space (nonmoving spikes). The spike surface thus obtains a fixed value of the spatial coordinate, e.g., $z_{\text{Spike}} = 0$. In this paper we have pushed the current numerical frontier in the context of the recurrence of *nonmoving spikes* by a numerically correct simulations of part of a chain of spike transitions that also involves low velocity spike solutions. The main challenge in this context is that low velocity spike solutions require numerical accuracy at super horizon scales.

In general, recurring spikes will not be spatially fixed, instead they will move, i.e., $z_{\text{Spike}} = z_{\text{Spike}}(t)$. These *moving spikes* are not directly described by the explicit spike solutions (29). However, it is possible that moving spikes *asymptotically freeze* in space which implies that the description of the recurrence of these spikes in terms of spike chains straightforwardly applies. There exists some heuristic evidence for asymptotically frozen spikes; e.g., this is suggested by the billiard picture where a "dominant wall" that has a hole in it at an isolated value of a spatial coordinate corresponds to a spatially frozen spike [52]. The question of asymptotic freezing is closely related to another unexplored area: Present numerical techniques are not sufficient to accurately describe the creation and the possible annihilation of spikes. This makes it difficult to guess whether the number of spikes that form remains finite, or whether, in general, an infinite number of spikes, possibly a dense set, is created in the asymptotic regime. It is doubtful whether a sound numerical investigation of this question is possible unless the numerics is supported by analytical insights.

There are many examples in general relativity that show that one must go beyond a given context in order to understand it, especially as regards asymptotics. This is particularly relevant as regards topology. For instance, Bianchi type I and II models are essential building blocks for the understanding of the singularities of the more general Bianchi models; it is important to note that this is irrespective of the fact that these Bianchi models have spatial topologies that are completely different from those of Bianchi types I and II. Yet another example is provided by the present paper: Understanding the singularities of $G_2$ models requires that one goes beyond $T^3$ topology, since the high and low velocity spike solutions do not admit such a topology. Special models like these provide local building blocks (where local may refer to the particle horizon scale) for the asymptotic description of more general models, or even generic ones.

The relationship between local and global issues deserves special attention. It is important to realize that the primary importance of the $G_2$ models as regards generic singularities is not the models themselves, but the crucial property that the $G_2$ equations are those of an invariant boundary subset of the general conformally Hubble-normalized state space (associated with the Einstein equations without symmetries), which we call the *partially local $G_2$ boundary.*[10] This subset is obtained by setting certain frame variables to zero to achieve $\boldsymbol{\partial}_1(*) = \boldsymbol{\partial}_2(*) = 0$ in the field equations, where $\boldsymbol{\partial}_1$ and $\boldsymbol{\partial}_2$ are Hubble-normalized spatial frame derivatives. As a consequence the constants of integration on this boundary subset in general depend on the spatial coordinates $x$ and $y$. The situation is therefore completely analogous to the relationship between the local boundary and the spatially homogeneous models. Since what survives of the $G_2$ models in the context of the general conformally Hubble-normalized state space is merely the equations (on a boundary subset), any global considerations, which may be of interest for the $G_2$ models themselves, are probably not particularly relevant in the general context (for general models there typically are other global considerations that are relevant). As regards generic singularities in the generic case for models without symmetries, it is therefore only *local $G_2$* results, within domains of dependence in the vicinity of the singularity, that are of relevance, e.g., for cosmic censorship. For further discussion on topological issues in the case of $G_2$ models, see Appendix A.

Going beyond the $G_2$ assumption and looking at models with fewer isometries does not only shift the attention to the partially local $G_2$ boundary, it leads to completely new challenges as well. Spike surfaces, within the context of the partially local $G_2$ boundary, are no longer planes, and they can intersect in curves that lead to different spike dynamics. Similarly, if one has no symmetries at all, spike curves may intersect at points, which again may lead to new spike dynamics. At present it is not known whether such

---

[10]The partially local $G_2$ boundary, previously referred to as a the partially silent boundary subset, yields, e.g., spiky behavior that is still associated with asymptotic silence, but also solutions with singularities that break asymptotic silence, which are characterized by the existence of directions in which particle horizons extend to infinity; see Ref. [67].

intersections persist or recur, or if they are transient and hence irrelevant asymptotically. Although weak numerical evidence suggests that intersections only occur momentarily, and hence that the BKL picture in combination with $G_2$ spike oscillations might capture all essential features of generic spacelike singularities. The above issues illustrate again that spike dynamics poses a formidable numerical and analytical challenge. It is clear that we are only beginning to understand the rich structure of generic singularities, and the underlying physical reasons for their existence and characteristics.

## ACKNOWLEDGMENTS

## APPENDIX A: $G_2$ MODELS AND TOPOLOGY

A $G_2$ model is a spacetime admitting two commuting spacelike Killing vectors. Such spacetimes are often assumed to be globally hyperbolic and the action to be effective on spacetime Cauchy hypersurfaces with two-dimensional principal orbits. Furthermore, many of the rigorous results concerns $G_2$ models with a compact Lie group that is identified with $T^2 = U(1) \times U(1)$, which results in the so-called ''$T^2$-symmetric spacetimes.'' By assuming compactness of the Cauchy hypersurfaces it follows that the topology has to be $T^3$, $S^2 \times S^1$, $S^3$, or one of quotient spaces of $S^3$, the Lens spaces $L(p; q)$ [72]. In the cases of $S^2 \times S^1$, $S^3$, and $L(p; q)$, the group action must have fixed points and hence the two ''twist constants'' $c_A = \mathrm{vol}_{abcd} X_1^a X_2^b \nabla^c X_A^d$, $A = 1, 2$, of the two commuting Killing vector fields $X_1$ and $X_2$ vanish (in general $c_A$ are nonzero spacetime constants if the Einstein vacuum equations are imposed [72,73]). In such cases the action is necessarily *orthogonally transitive* (OT) [7], i.e., the 2-spaces orthogonal to the group orbits are surface forming.

The spatially compact topology that is of particular interest in the context of generic singularities is $T^3 = S^1 \times T^2$ (and its covering $\mathbb{R} \times T^2$), because in this case the twist constants do not vanish in general, i.e., in the $T^3$ case, $c_1 = c_2 = 0$ is a restriction. The (standard) $T^3$ case arises from the $\mathbb{R} \times T^2$ case by identifying $\{0\} \times T^2$ and $\{2\pi\} \times T^2$ by means of periodic boundary conditions for the metric and the extrinsic curvature. (The corresponding OT models are the $T^3$ Gowdy models [26].) It is also possible to consider nontrivial torus bundles over $S^1$, which correspond to identifying $\{0\} \times T^2$ and $\{2\pi\} \times T^2$ through nontrivial $SL(2, \mathbb{Z})$

transformations. In this case, the action of $T^2$ is global on the covering space $\mathbb{R} \times T^2$ but merely local on $T^3$ and the metric and the extrinsic curvature satisfy nontrivial boundary conditions; see, e.g., Ref. [74], where specializations to spatially homogeneous Bianchi models is also discussed.

It is possible to without loss of generality assume the vanishing of one of the twist constants. If $c_1 c_2 \neq 0$ there are linear combinations $X_1'$ and $X_2'$ of $X_1$ and $X_2$, which are again Killing vector fields, such that the associated twist constants are $c_x = 0$ and $c_y \neq 0$. By introducing local coordinates such that $X_1' \equiv \partial_x$ and $X_2' \equiv \partial_y$ [unless $X_1$, $X_2$ and $X_1'$, $X_2'$ are related by an $SL(2, \mathbb{Z})$ transformation, $x$ and $y$ are not standard coordinates on $T^2$, but this does not affect the equations; see Ref. [72]], we obtain the second form of the metric in (1), which is easily seen to coincide with the metric in Refs. [32,60]. In the spatially compact case, these functions are periodic in $z$ [or, in the case of a nontrivial torus bundle, satisfy boundary conditions derived from the particular $SL(2, \mathbb{Z})$ identification]. In terms of the metric functions, cf. (1), and the area density $R$, the twist constants are represented by

$$c_x = 0 \Leftrightarrow -\partial_{x^0} \bar{n}_2 + \bar{n}_1 \partial_{x^0} \bar{n}_3 = \partial_{x^0} n_2 - n_3 \partial_{x_0} n_1 = 0, \quad \text{(A1a)}$$

$$c_y = R^3 e^{2b^1 + b^3} N^{-1} \partial_{x^0} n_3 = e^{-b^1 - 3b^2 + b^3} N^{-1} \partial_{x^0} n_3. \quad \text{(A1b)}$$

and hence if and only if $c_x = 0$ then $R_2 = 0$, as follows from Eq. (B1f) below. In area time gauge (3) the metric takes the form (4), where $\bar{\alpha}$ satisfies the equation $\partial_t \bar{\alpha} = e^{2b^2 - 2b^3} \bar{\alpha}^2 c_y^2$ see Ref. [60], and $c_y$ becomes $c_y = -e^{-2b^2 + 2b^3} \bar{\alpha}^{-1/2} \partial_t n_3$. From this, and Eq. (A1), it follows that $\bar{\alpha}$ and $n_2$, $n_3$ become independent of time in the OT case, which is characterized by vanishing twist constants. By using the coordinate freedom $x \mapsto x + f_1(z)$, $y \mapsto y + f_2(z)$, $z \mapsto f_3(z)$ and redefining $b^3$ it is possible to set $\bar{\alpha} \equiv 1$, which corresponds to a lapse function (5), and $n_2 = n_3 \equiv 0$. Note that setting $\bar{\alpha} \equiv 1$ is impossible in the general case with $c_y \neq 0$ as long as the area time gauge is enforced; on the other hand, abandoning (3) makes the ''conformal gauge'' (or ''null cone gauge'' [64]) $\bar{\alpha} \equiv 1$ possible [60].

## APPENDIX B: METRIC VARIABLES AND HUBBLE-NORMALIZED VARIABLES IN THE $G_2$ CASE

In the $G_2$ case, the general relations of Appendix A of Ref. [51] reduce to the following relationship between the metric variables $b^1$, $b^2$, $b^3$, $n_1$, $n_2$, $n_3$, and the Hubble variable $H$ and the conformally Hubble-normalized state space variables:

$$E_3 = H^{-1} \exp(b^3),$$

$$r = -H^{-2} \exp(b^3) \partial_z H,$$

$$A = r + \frac{1}{2} H^{-1} \exp(b^3) \partial_z (b^1 + b^2),$$

$$H = -\frac{1}{3} N^{-1} \partial_{x^0}(b^1 + b^2 + b^3), \quad \text{(B1a)}$$

$$\dot{U} = -r + (NH)^{-1} \exp(b^3) \partial_z N, \quad \text{(B1b)}$$

$$q = -1 - N^{-1} H^{-2} \partial_{x^0} H. \quad \text{(B1c)}$$

For simplicity we have set $E_3 = E_3{}^3$, $A = A_3$, $r = r_3$, and $\dot{U} = \dot{U}_3$. These quantities refer to an Iwasawa frame; functions depend on $x^0$ and $z$ alone. Furthermore,

$$\Sigma_\alpha = -1 - (NH)^{-1}\partial_{x^0}(b^\alpha) \qquad (\alpha = 1, 2, 3), \tag{B1d}$$

$$R_1 = -\Sigma_{23} = -\frac{1}{2}(NH)^{-1}\exp(b^3 - b^2)\partial_{x^0}(n_3), \tag{B1e}$$

$$R_2 = \Sigma_{31} = \frac{1}{2}(NH)^{-1}\exp(b^3 - b^1)[\partial_{x^0}(n_2) - n_3\partial_{x^0}(n_1)], \tag{B1f}$$

$$R_3 = -\Sigma_{12} = -\frac{1}{2}(NH)^{-1}\exp(b^2 - b^1)\partial_{x^0}(n_1), \tag{B1g}$$

$$N_1 = H^{-1}\exp(b^2 + b^3 - b^1)\partial_z(n_1), \tag{B1h}$$

$$N_{12} = \frac{1}{2}H^{-1}\exp(b^3)\partial_z(b^1 - b^2). \tag{B1i}$$

Adapting the spatial coordinates to achieve the vanishing of the first twist constant leads to $\partial_{x^0}n_2 - n_3\partial_{x^0}n_1 = 0$, see (A1a), and thus $R_2 = 0$. In area time gauge, the sum $b^1 + b^2$ does not depend on $z$, hence $A \equiv r$ in that case. The lapse $N$ is unspecified in general; for OT models in area time gauge, however, we have $N = -\exp(-b^1 - b^2 - b^3)$, see (5).

## APPENDIX C: VACUUM FIELD EQUATIONS IN THE $G_2$ CASE

The vacuum field equations for the conformally Hubble-normalized variables in the $G_2$ case are conveniently divided into decoupled equations and a coupled system of evolution equations and constraints.

The *decoupled equations* (for the metric variables and the Hubble scalar) read

$$\boldsymbol{\partial}_0 b^\alpha = -(1 + \Sigma_\alpha) \quad (\alpha = 1, 2, 3), \qquad \boldsymbol{\partial}_0 n_1 = -2R_3\exp(b^2 - b^1), \tag{C1a}$$

$$\boldsymbol{\partial}_0 n_2 = n_3\boldsymbol{\partial}_0 n_1, \qquad \boldsymbol{\partial}_0 n_3 = -2R_1\exp(b^3 - b^2), \tag{C1b}$$

$$\boldsymbol{\partial}_0 H = -(1 + q)H, \tag{C1c}$$

$$\boldsymbol{\partial}_3(b^1 - b^2) = 2N_{12}, \qquad \boldsymbol{\partial}_3(b^1 + b^2) = 2(A - r), \tag{C1d}$$

$$\boldsymbol{\partial}_3 n_1 = N_1\exp(b^1 - b^2), \qquad \boldsymbol{\partial}_3 N = (\dot{U} + r)N, \tag{C1e}$$

$$\boldsymbol{\partial}_3 H = -rH, \tag{C1f}$$

where the conformal frame vectors are

$$\boldsymbol{\partial}_0 \equiv (NH)^{-1}\partial_{x^0}, \qquad \boldsymbol{\partial}_3 \equiv E_3\partial_z. \tag{C2}$$

The *coupled evolution equations* for the conformally Hubble-normalized variables are

$$\boldsymbol{\partial}_0 E_3 = (q - \Sigma_3)E_3, \tag{C3a}$$

$$\boldsymbol{\partial}_0 \Sigma_1 = -(2 - q)\Sigma_1 + 2R_3^2 - {}^3S_1 - \frac{1}{3}(\boldsymbol{\partial}_3 + A + 3N_{12})(\dot{U} + 2r) - \frac{1}{3}(\dot{U}^2 - 2r^2), \tag{C3b}$$

$$\boldsymbol{\partial}_0 \Sigma_2 = -(2 - q)\Sigma_2 - 2R_3^2 + 2R_1^2 - {}^3S_2 - \frac{1}{3}(\boldsymbol{\partial}_3 + A - 3N_{12})(\dot{U} + 2r) - \frac{1}{3}(\dot{U}^2 - 2r^2), \tag{C3c}$$

$$\boldsymbol{\partial}_0 \Sigma_3 = -(2 - q)\Sigma_3 - 2R_1^2 - {}^3S_3 + \frac{2}{3}(\boldsymbol{\partial}_3 + A)(\dot{U} + 2r) + \frac{2}{3}(\dot{U}^2 - 2r^2), \tag{C3d}$$

$$\boldsymbol{\partial}_0 R_1 = -(2 - q + \Sigma_2 - \Sigma_3)R_1, \tag{C3e}$$

$$\boldsymbol{\partial}_0 R_3 = -(2 - q + \Sigma_1 - \Sigma_2)R_3 + {}^3S_{12} - \frac{1}{2}N_1(\dot{U} + 2r), \tag{C3f}$$

$$\boldsymbol{\partial}_0 A = (q - \Sigma_3)A + \frac{1}{2}(\boldsymbol{\partial}_3 + \dot{U})(2q + \Sigma_3), \tag{C3g}$$

$$\boldsymbol{\partial}_0 N_1 = (q + 2\Sigma_1)N_1 - 2(\boldsymbol{\partial}_3 + \dot{U} + 2N_{12})R_3, \tag{C3h}$$

$$\boldsymbol{\partial}_0 N_{12} = (q - \Sigma_3)N_{12} - \frac{1}{2}(\boldsymbol{\partial}_3 + \dot{U})(\Sigma_1 - \Sigma_2). \tag{C3i}$$

The *coupled constraint equations* take the form

$$0 = 1 - \Sigma^2 - \Omega_k - \frac{1}{3}(2\partial_3 - 4A + r)r, \qquad \text{(C4a)}$$

$$0 = (\partial_3 - 3A + 2r + N_{12})R_1, \qquad \text{(C4b)}$$

$$0 = 2r + (\partial_3 - 3A + 2r)\Sigma_3 + (\Sigma_1 - \Sigma_2)N_{12} + N_1 R_3. \qquad \text{(C4c)}$$

In these equations we have used the abbreviations

$$\Omega_k = \frac{1}{12}(N_1^2 + 4N_{12}^2) - \frac{1}{3}(2\partial_3 - 3A)A, \qquad \text{(C5a)}$$

$${}^3\mathcal{S}_1 = \frac{2}{3}(N_1^2 + N_{12}^2) - 2N_{12}A - \frac{1}{3}\partial_3(A - 3N_{12}), \qquad \text{(C5b)}$$

$${}^3\mathcal{S}_2 = -\frac{1}{3}(N_1^2 - 2N_{12}^2) + 2N_{12}A - \frac{1}{3}\partial_3(A + 3N_{12}), \qquad \text{(C5c)}$$

$${}^3\mathcal{S}_3 = -\frac{1}{3}(N_1^2 + 4N_{12}^2) + \frac{2}{3}\partial_3 A, \qquad \text{(C5d)}$$

$${}^3\mathcal{S}_{12} = -\frac{1}{2}(\partial_3 - 2N_{12} - 2A)N_1, \qquad \text{(C5e)}$$

$$q = 2\Sigma^2 - \frac{1}{3}[\partial_3 + \dot{U} - 2(A - r)](\dot{U} + r), \qquad \text{(C5f)}$$

$$\Sigma^2 = \frac{1}{6}(\Sigma_1^2 + \Sigma_2^2 + \Sigma_3^2 + 2R_1^2 + 2R_3^2). \qquad \text{(C5g)}$$

The conformally Hubble-normalized equations are not the most useful equations in the $G_2$ context. Instead one can adapt to the special structure of these models and use, e.g., conformally area-expansion-normalized variables; see Refs. [54,64]. However, since we are interested in how the $G_2$ case fits into the general context without symmetries we have focused on the conformal Hubble-normalized approach in this paper.

## APPENDIX D: OT MODELS: ASYMPTOTIC VELOCITY DOMINANCE

In this section we give a brief overview of existing rigorous results for $T^3$ Gowdy vacuum models. The metric (45) in area time gauge is sometimes written in the form

$$ds^2 = -e^{(t-\lambda)/2}(-e^{-2t}dt^2 + dz^2) + e^{P-t}(dx + Qdy)^2 + e^{-P-t}dy^2, \qquad \text{(D1)}$$

see, e.g., Eq. (15) in Ref. [39]. There exists a number of diagnostic tools connected with (D1). In particular one can define kinetic and potential energy densities according to [70]

$$\mathcal{K} = \mathcal{K}(t, z) = (P_{,t})^2 + (e^P Q_{,t})^2,$$
$$\mathcal{P} = \mathcal{P}(t, z) = (e^{-t}P_{,z})^2 + (e^{P-t}Q_{,z})^2, \qquad \text{(D2)}$$

and a *velocity* $v$ as the square root of $\mathcal{K}$ (hence more appropriately referred to as a speed). The quantities $\mathcal{K}$, $\mathcal{P}$, and $v$ are intimately connected with the Hubble-normalized variables. In Ref. [75], it was noted that the velocity $v$ is

$$v = v(t, z) = \sqrt{\mathcal{K}} = \frac{\sqrt{\frac{1}{4}(\Sigma_1 - \Sigma_2)^2 + R_3^2}}{1 - \frac{1}{2}\Sigma_3}$$
$$= \sqrt{3}\frac{\sqrt{\Sigma^2 - \frac{1}{4}\Sigma_3^2}}{1 - \frac{1}{2}\Sigma_3}. \qquad \text{(D3)}$$

We also obtain

$$\tilde{p}_1 = \frac{2(1 - P_{,t})}{3 + \mathcal{K} + \mathcal{P}}, \qquad \tilde{p}_2 = \frac{2(1 + P_{,t})}{3 + \mathcal{K} + \mathcal{P}}, \qquad \tilde{p}_3 = \frac{-1 + \mathcal{K} + \mathcal{P}}{3 + \mathcal{K} + \mathcal{P}}, \qquad \text{(D4a)}$$

$$R_3 = 6\frac{e^P Q_{,t}}{3 + \mathcal{K} + \mathcal{P}}, \qquad N_1 = 12\frac{e^{P-t}Q_{,z}}{3 + \mathcal{K} + \mathcal{P}}, \qquad N_{12} = -6\frac{e^{-t}P_{,z}}{3 + \mathcal{K} + \mathcal{P}} \qquad \text{(D4b)}$$

from which we infer that

$$\tilde{p}_1^2 + \tilde{p}_2^2 + \tilde{p}_3^2 = 1 - 8\frac{e^{2P}Q_{,t}^2 + \mathcal{P}}{(3 + \mathcal{K} + \mathcal{P})^2},$$
$$\Sigma^2 = 1 - 12\frac{\mathcal{P}}{(3 + \mathcal{K} + \mathcal{P})^2}. \qquad \text{(D4c)}$$

A considerable part of the analytic rigorous work on spacelike singularities has been influenced by the work by Eardley *et al.* [76], which has resulted in a focus on *asymptotic velocities*. The term asymptotic velocity refers to the limit

$$v_\infty = v_\infty(z) = \lim_{t\to\infty} v(t, z) = \lim_{t\to\infty}\sqrt{\mathcal{K}(t, z)} = |2\check{u} + 1|. \qquad \text{(D5)}$$

In the context of the $T^3$ Gowdy models, the existence of this limit has been proved. Specifically, for each smooth solution $(P, Q)$, $v_\infty$ is an upper semicontinuous function of $z$ [70]. Furthermore, $e^{2P}Q_{,t}^2$ and $\mathcal{P}$ converge to zero as $t \to \infty$ and $P_{,t}^2 \to v_\infty^2$ ($t \to \infty$). This holds not merely pointwise in $z$ but uniformly on the shrinking particle horizons $[z - e^{-t}, z + e^t]$ associated with a $z = $ const time line; we refer to our discussion of particle horizons in Sec. IV. Evidently, the spatial topology is irrelevant in this context. Following Moncrief and coworkers, the asymptotic velocity $v_\infty$ has been used extensively as a diagnostic tool see, e.g., Refs. [28,36,39,70,77,78]. To resolve the ambiguity in the limit of $P_{,t}$, following Refs. [35,36] one may define the asymptotic velocity component

$$k = \lim_{t\to\infty} P_{,t} = \lim_{t\to\infty} \frac{\Sigma_1 - \Sigma_2}{2(1 - \frac{1}{2}\Sigma_3)} = 2\check{u} + 1, \quad \text{(D6)}$$

i.e., $|k| = v_\infty$; it follows that $0 < k < 1$ corresponds to $-\frac{1}{2} < \check{u} < 0$, i.e., to the stable sector (312).

The convergence statements are commonly subsumed under the term "asymptotic velocity dominance," and the existence of the limit (D5) is referred to as convergence of solutions to an asymptotically velocity dominated state. As a consequence of (D4), however, the convergence statements simply mean that each solution converges to a generalized Kasner metric with a semicontinuous Kasner parameter $\check{u} = \check{u}(z)$.

Building on Ref. [28] and the results of Rendall and coworkers [36,37], Ringström proved that in the $T^3$ Gowdy case solutions $(P, Q)$ with $0 < k < 1$ ($\Rightarrow k = v_\infty$) possess asymptotic expansions of the form

$$P(t, z) = v_\infty(z)t + \phi(z) + u(t, z),$$
$$Q(t, z) = q(z) + e^{-2v_\infty(z)t}(\psi(z) + w(t, z)), \quad \text{(D7)}$$

where $u$ and $w$ and its derivatives converge to zero exponentially; see Prop. 1.5 in Ref. [70] for the precise statement. [The assumption $0 < k(z_0) < 1$ for some $z_0$ is sufficient to obtain smoothness of $v_\infty$ and uniform expansions of the type (D7) in a neighborhood of $z_0$.] Note that the expansion (D7) represents the convergence of solutions to the stable sector of the Kasner circle. In Refs. [78–80] criteria on initial data have been derived that guarantee the assumption $0 < k < 1$ on the asymptotic velocity. By these theorems, the heuristic reasoning of Sec. IV B that solutions that are sufficiently close to a generalized Kasner metric on the stable sector converge to the stable sector is made rigorous for the $T^3$ Gowdy models.

There also exist solutions with asymptotic expansions of the type (D7) where, however, the asymptotic velocity $v_\infty$ is discontinuous, thus exhibiting a true *spike* in the nomenclature of Ref. [39]. Here the term true refers to the nonuniform convergence of scalar functions, e.g., the Hubble-normalized Kretschmann scalar, to a discontinuous limit (false spikes, which we refrain from discussing, possess a discontinuous $k$, but $v_\infty$ and the curvature scalars are continuous). Alternatively, these solutions are said to possess a permanent spike. The explicit low velocity spike solutions (36) fall into this category, while the explicit high velocity spike solution (35) possess a constant (and thus continuous) asymptotic velocity. However, we strongly emphasize that the "permanence" of low velocity spike solutions, i.e., convergence to a discontinuous limit, is true *in the OT context only*. As seen in Sec. V, spikes are not permanent but transient and recurring features in the general $G_2$ case.

In the Gowdy literature the question of whether a velocity is high or low usually refers to the asymptotic velocity $v_\infty$. However, the explicit spike solutions (29) do not easily fall into the "high or low" asymptotic velocity scheme: For the

explicit high velocity solutions the limit $v_\infty$ is an arbitrary positive number; for the explicit low velocity solutions the limit is in the interval $(1, 2)$ for the spike time lines and in the interval $(0, 1)$ for the $z \neq 0$ time lines. In the context of the explicit spike solutions it is thus preferable to classify solutions in terms of their limit $t \to -\infty$; the corresponding (anti)asymptotic velocity (as $t \to -\infty$) is in the interval $(2, 3)$ for the explicit low velocity spike solutions and in the interval $(3, \infty)$ for the explicit high velocity spike solutions, thus motivating the present nomenclature for the spike solutions.

The usefulness of $v$ in the characterization of the behavior of OT models is indisputable since it captures essential aspects of the dynamics of solutions. However, it should not come as a surprise that $v$ fails to capture *all* aspects of the dynamics. Furthermore, the role of $v$ is diminished when we go beyond the OT case where $v_\infty$ does not even exist since $v$ does not converge; see Sec. V. A clearer picture that is also applicable to the general case is obtained when we do not restrict ourselves to one particular degree of freedom, but instead consider projections of the Hubble-normalized state vector onto the 2-dimensional space spanned by $(\Sigma_1, \Sigma_2, \Sigma_3)$. With hindsight, and with issues concerning generic singularities and cosmic censorship as ultimate goals, we find that there is room for improvement concerning the terminology that is used in much of the literature.

## APPENDIX E: EVOLUTION OF SPIKE WIDTHS

In this section of the Appendix, we show the result given in Eq. (48). Consider Eq. (C3f). In area time gauge, since (B1c) implies that $A \equiv r$, we have

$$\mathcal{N}^{-1}\partial_t R_3 = -(2 - q + \Sigma_1 - \Sigma_2)R_3 - \frac{1}{2}\boldsymbol{\partial}_3 N_1$$
$$+ N_1 N_{12} - \frac{1}{2}N_1\dot{U}, \quad \text{(E1)}$$

where $\dot{U} = \boldsymbol{\partial}_3 \log(-\mathcal{N})$ and where the Hubble-normalized lapse $\mathcal{N}$ is given by

$$\mathcal{N} = NH = -\frac{1}{2 - \Sigma_3}, \quad \text{(E2)}$$

which follows from $b^1 + b^2 = t$ and (B1d) by using that $\Sigma_3 = -\Sigma_1 - \Sigma_2$. Making use of (C5f) and the constraint (C4a) Eq. (C3d) turns into

$$\mathcal{N}^{-1}\partial_t\Sigma_3 = (2 - q)(2 - \Sigma_3) - 2R_1^2. \quad \text{(E3)}$$

Therefore, in the OT case, where $R_1 \equiv 0$, we find that

$$\mathcal{N}^{-1}\partial_t\mathcal{N} = (2 - q)\mathcal{N}. \quad \text{(E4)}$$

Accordingly, Eq. (E1) yields

$$\mathcal{N}^{-2}\partial_t(\mathcal{N}R_3) = -(\Sigma_1 - \Sigma_2)R_3 - \frac{1}{2}E_3\partial_z N_1$$
$$+ N_1 N_{12} - \frac{1}{2}N_1 E_3 \partial_z \log(-\mathcal{N}). \quad \text{(E5)}$$

Furthermore, from (C3a) and (E4) we obtain

$$\partial_t(\mathcal{N}E_3) = -\mathcal{N}E_3, \quad \text{(E6)}$$

which entails that $\mathcal{N}E_3 = -ke^{-t}$ for some $k = k(z)$; we set $\kappa = k(0)$.

Consider an OT solution $\mathcal{S}$ that is an approximate OT spike chain with spike surface $z = 0$ and symmetric functions; i.e., $\Sigma_1$, $\Sigma_2$, $\Sigma_3$, and $R_3$ are even and $N_1$, $N_{12}$ are odd. We evaluate (E5) at the spike surface $z = 0$ to obtain

$$\partial_z N_1|_{z=0} = -2(\mathcal{N}E_3)^{-1}|_{z=0}(\mathcal{N}^{-1}\partial_t(\mathcal{N}R_3)$$
$$+ (\Sigma_1 - \Sigma_2)\mathcal{N}R_3)|_{z=0}. \quad \text{(E7)}$$

Insertion into (47) yields an expression for the spike coordinate width $c_z$ according to

$$c_z = (\mathcal{N}E_3)^{-1}|_{z=0} \times \text{function}\,(\text{spike surface orbit } z = 0).$$
$$\text{(E8)}$$

Note that the spike surface orbits at $z = 0$ are independent of the width of the (approximate) spike transition. For an explicit spike solution with width $\check{c}$ and time offset $-\check{t}$, i.e., (29) where $z$ is replaced by $\check{c}z$ and $t$ by $t - \check{t}$, we have $\mathcal{N}E_3 = -\check{c}^{-1}e^{-(t-\check{t})}$, which follows from (40) and (B1a), while the function of the spike surface orbits yields $-e^{-(t-\check{t})}$.

Suppose that the approximate OT spike chain is approximated in some time interval by an exact spike transition with parameter $\check{u}_0$, (inverse) width $c_0$, and time offset $-t_0$; hence, by (E8),

$$c_0 = -\kappa^{-1}e^t e^{-(t-t_0)}. \quad \text{(E9)}$$

At a (much) later time, when the solution is approximated by the subsequent $\mathcal{T}_{\text{Hi}}$ of the OT chain; the Kasner parameter is $\check{u}_1 = \check{u}_0 - 2$, the (inverse) width is $c_1$ and the time offset is $-t_1$ (where $t_1 \gg t_0$). According to (E8) and (E9) we have

$$c_1 = -\kappa^{-1}e^t e^{-(t-t_1)} = c_0 e^{t-t_0} e^{-(t-t_1)} = c_0 e^{t_1-t_0}, \quad \text{(E10)}$$

i.e., the (inverse) coordinate width increases by a factor of $e^{t_1-t_0}$. This establishes (48).

[1] E. M. Lifshitz and I. M. Khalatnikov, Adv. Phys. **12,** 185 (1963).
[2] V. A. Belinskiĭ, I. M. Khalatnikov, and E. M. Lifshitz, Adv. Phys. **19,** 525 (1970).
[3] V. A. Belinskiĭ, I. M. Khalatnikov, and E. M. Lifshitz, Adv. Phys. **31,** 639 (1982).
[4] I. M. Khalatnikov, E. M. Lifshitz, K. M. Khanin, L. N. Shur, and Y. G. Sinai, J. Stat. Phys. **38,** 97 (1985).
[5] J. D. Barrow, Phys. Rep. **85,** 1 (1982).
[6] D. F. Chernoff and J. D. Barrow, Phys. Rev. Lett. **50,** 134 (1983).
[7] J. Wainwright and G. F. R. Ellis, *Dynamical Systems in Cosmology* (Cambridge University Press, Cambridge, 1997).
[8] A. A. Coley, *Dynamical Systems and Cosmology* (Kluwer Academic Publishers, Dordrecht, 2003).
[9] Y. Aizawa, N. Koguro, and I. Antoniou, Prog. Theor. Phys. **98,** 1225 (1997).
[10] B. K. Berger, Living Rev. Relativity **5,** 6 (2002).
[11] Y. Elskens and M. Henneaux, Nucl. Phys. **B290,** 111 (1987).
[12] C. Cherubini, D. Bini, M. Bruni, and Z. Perjes, Classical Quantum Gravity **22,** 1763 (2005).
[13] D. Hobill, A. Burd, and A. Coley, *Deterministic Chaos in General Relativity* (Plenum Press, New York, 1994).
[14] N. J. Cornish and J. J. Levin, Phys. Rev. D **55,** 7489 (1997).
[15] N. J. Cornish and J. J. Levin, Phys. Rev. Lett. **78,** 998 (1997).
[16] S. E. Rugh, Cand. Scient. thesis, Niels Bohr Institute, København, 1990.

[17] A. E. Motter and P. S. Letelier, Phys. Lett. A **285,** 127 (2001).
[18] R. Benini and G. Montani, Phys. Rev. D **70,** 103527 (2004).
[19] G. Montani, M. V. Battisti, R. Benini, and G. Imponente, Int. J. Mod. Phys. A **23,** 2353 (2008).
[20] T. Damour and O. M. Lecian, Phys. Rev. D **83,** 044038 (2011).
[21] T. Damour and O. M. Lecian, arXiv:1103.0179.
[22] A. A. Kirillov and A. A. Kochnev, Pis'ma Zh. Eksp. Teor. Fiz. **46,** 435 (1987) [JETP Lett. **46,** 435 (1987)].
[23] G. Montani, Ph.D. thesis, Universita di Roma, Facolta di Fisica, 1992.
[24] V. A. Belinskiĭ, Pis'ma Zh. Eksp. Teor. Fiz. **56,** 437 (1992).
[25] R. H. Gowdy, Phys. Rev. Lett. **27,** 826 (1971).
[26] R. H. Gowdy, Ann. Phys. (Berlin) **83,** 203 (1974).
[27] B. K. Berger and V. Moncrief, Phys. Rev. D **48,** 4676 (1993).
[28] B. Grubišić and V. Moncrief, Phys. Rev. D **47,** 2371 (1993).
[29] B. K. Berger and V. Moncrief, Phys. Rev. D **58,** 064023 (1998).
[30] B. K. Berger, D. Garfinkle, J. Isenberg, V. Moncrief, and M. Weaver, Mod. Phys. Lett. A **13,** 1565 (1998).
[31] B. K. Berger and D. Garfinkle, Phys. Rev. D **57,** 4767 (1998).
[32] B. K. Berger, J. Isenberg, and M. Weaver, Phys. Rev. D **64,** 084006 (2001).
[33] S. D. Hern, Ph.D. thesis, University of Cambridge, 1999 [arXiv:gr-qc/0004036].

[34] S. D. Hern and J. M. Stewart, Classical Quantum Gravity **15**, 1581 (1998).

[35] A. D. Rendall and M. Weaver, Classical Quantum Gravity **18**, 2959 (2001).

[36] S. Kichenassamy and A. D. Rendall, Classical Quantum Gravity **15**, 1339 (1998).

[37] A. D. Rendall, Classical Quantum Gravity **17**, 3305 (2000).

[38] D. Garfinkle and M. Weaver, Phys. Rev. D **67**, 124009 (2003).

[39] H. Ringström, Living Rev. Relativity **13**, 2 (2010), http://www.livingreviews.org/lrr-2010-2.

[40] J. Wainwright and L. Hsu, Classical Quantum Gravity **6**, 1409 (1989).

[41] H. Ringström, Classical Quantum Gravity **17**, 713 (2000).

[42] H. Ringström, Ann. Inst. Henri Poincaré **2**, 405 (2001).

[43] J. M. Heinzle and C. Uggla, Classical Quantum Gravity **26**, 075015 (2009).

[44] J. M. Heinzle and C. Uggla, Classical Quantum Gravity **26**, 075016 (2009).

[45] M. Reiterer and E. Trubowitz, arXiv:1005.4908v2.

[46] F. Béguin, Classical Quantum Gravity **27**, 185005 (2010).

[47] S. Liebscher, J. Härterich, K. Webster, and M. Georgi, Commun. Math. Phys. **305**, 59 (2011).

[48] S. Liebscher, A. D. Rendall, and S. B. Tchapnda, arXiv:1207.2655.

[49] C. Uggla, H. van Elst, J. Wainwright, and G. F. R. Ellis, Phys. Rev. D **68**, 103502 (2003).

[50] N. Röhr and C. Uggla, Classical Quantum Gravity **22**, 3775 (2005).

[51] J. M. Heinzle, C. Uggla, and N. Röhr, Adv. Theor. Math. Phys. **13**, 293 (2009).

[52] T. Damour, M. Henneaux, and H. Nicolai, Classical Quantum Gravity **20**, R145 (2003).

[53] L. Andersson, H. van Elst, W. C. Lim, and C. Uggla, Phys. Rev. Lett. **94**, 051101 (2005).

[54] W. C. Lim, Ph. D. thesis, University of Waterloo, 2004 [arXiv:gr-qc/0410126].

[55] D. Garfinkle, Phys. Rev. Lett. **93**, 161101 (2004).

[56] W. C. Lim, Classical Quantum Gravity **25**, 045014 (2008).

[57] W. C. Lim, L. Andersson, D. Garfinkle, and F. Pretorius, Phys. Rev. D **79**, 123526 (2009).

[58] A. Coley and W. C. Lim, Phys. Rev. Lett. **108**, 191101 (2012).

[59] J. Wainwright, J. Phys. A **14**, 1131 (1981).

[60] B. K. Berger, P. T. Chruściel, J. Isenberg, and V. Moncrief, Ann. Phys. (Berlin) **260**, 117 (1997).

[61] H. Andréasson, A. D. Rendall, and M. Weaver, Commun. Partial Differ. Equ. **29**, 237 (2005).

[62] A. D. Rendall, *Partial Differential Equation in General Relativity* (Oxford University Press, Oxford, 2008).

[63] J. Isenberg and M. Weaver, Classical Quantum Gravity **20**, 3783 (2003).

[64] H. van Elst, C. Uggla, and J. Wainwright, Classical Quantum Gravity **19**, 51 (2002).

[65] B. Carter, in *Black Holes*, edited by C. Dewitt and B. S. DeWitt (Gordon and Breach, New York, 1973).

[66] J. Wainwright, J. Phys. A: Math. Gen. **12**, 2015 (1979).

[67] W. C. Lim, C. Uggla, and J. Wainwright, Classical Quantum Gravity **23**, 2607 (2006).

[68] P. Sandin and C. Uggla, Classical Quantum Gravity **27**, 025013 (2010).

[69] J. M. Heinzle and H. Ringström, Classical Quantum Gravity **26**, 145001 (2009).

[70] H. Ringström, Commun. Pure Appl. Math. **59**, 977 (2006).

[71] J. M. Heinzle and C. Uggla, "Generic spacelike singularities: Attractors, chains, and statistics" (unpublished).

[72] P. T. Chruściel, Ann. Phys. (Berlin) **202**, 100 (1990).

[73] R. Geroch, J. Math. Phys. (N.Y.) **13**, 394 (1972).

[74] A. D. Rendall, J. Geom. Phys. **62**, 569 (2012).

[75] L. Andersson, H. van Elst, and C. Uggla, Classical Quantum Gravity **21**, S29 (2004).

[76] D. Eardley, E. Liang, and R. Sachs, J. Math. Phys. (N.Y.) **13**, 99 (1972).

[77] J. Isenberg, M. Jackson, and V. Moncrief, J. Math. Phys. (N.Y.) **31**, 517 (1990).

[78] M. Chae and P. T. Chruściel, Commun. Pure Appl. Math. **57**, 1015 (2004).

[79] H. Ringström, Classical Quantum Gravity **21**, S305 (2004).

[80] H. Ringström, Math. Proc. Cambridge Philos. Soc. **136**, 485 (2004).